ዘይሎ

ISSN: 0514-6216

የኢትዮጵያ መሐንዲሶችና አርኪቴክቶች መጽሔት

Indexed on
AJOL

zede

Journal of Ethiopian Engineers and Architects

35 ጥቅምት ፳፻፱
October 2017

Annual Publication of the Addis Ababa Institute of Technology
Addis Ababa University

□□
የኢትዮ□ያ መሐንዲሶችና አርኪቴክቶች መፅሔት

Zede

Journal of Ethiopian Engineers and Architects

□ዙቋቋመ□· ፲፱፻፶፮	ጥቅምት ፳፻፲	**35**	□ :ሣ፡ቁ፡ አዲስአበባ
Established 1963	October 2017		P.O.Box 385
AddisAbaba			

Publisher

Addis Ababa University
AAU Printing Press
P.O.Box 1178
Addis Ababa
Ethiopia

Postal Address
Addis Ababa University
P.O.Box 385
Addis Ababa
Ethiopia
Websit
www.aait.edu.et/zede
Email: zede@aait.edu.et

CONTENTS **Pages**

Notes to Contributors to the Journal

ZEDE is a scientific journal on engineering science and application, produced under the auspices of the Addis Ababa Institute of Technology, Addis Ababa University. The main objective of the journal is to publish research articles, findings and discussions on engineering sciences, technology and architecture thereby assisting in the dissemination of engineering knowledge and methodologies in solving engineering problems. Technical Notes of significant contribution may be considered for publication.

Original papers for publication in the journal should be submitted in triplicate to the Editor-in-Chief, P.O. Box 385, Addis Ababa, Ethiopia. All articles submitted for publication in the journal should comply with the following requirements:

1. ***Title of Paper***: The title of the paper should be phrased to include only key words and must have a length of not exceeding *80* characters including spaces.

2. ***Format of Manuscript***: The manuscript should be double-spaced in *A-4* sized paper typed in a word processor compatible *with MS* Word. Margins of *25 mm* should be used on all sides of the paper.

3. ***Length of Article***: The length of the article should not exceed word equivalent of 6000 words, or *20* pages, double spaced using font size *12* typed in Times New Roman.

4. ***Author's Affiliation***: The author's full name, institutional affiliation and rank, if applicable, must appear on the paper.

5. ***Abstract***: All articles submitted must include an abstract of length not exceeding *200* words in *italics*.

6. ***Keywords***: All articles submitted must include Keywords not exceeding 6 in number.

7. ***Style of Writing***: It is recommended that third person pronoun/s be used when referring to author/s.

8. ***Illustrations***: Figures should be drawn in black, at a size with a *50%* reduction to fit in *160 mm* width of journal. Photographs should be submitted as glossy prints. Explanations and descriptions must be placed in the text and not within figures. All figures must include numbered captions. See example: Figure 1 Typical creep strain versus time curve

9. ***Tables***: Tables must be numbered in the same order as cited in the text. Explanations of tables must appear in the text.

10. ***Equations***: Equations numbers should be right-justified. See example:

$$u(x, y) = -y\theta(x) \qquad (1)$$

11. ***References***: References in the body of the Article should be cited at the end of the paper by placing a reference number in square brackets and should be arranged sequentially as they appear in the text. Ethiopian names may be given in direct order, i.e. given name followed by father's name. All main words in titles (papers, books, reports) should be initialized by capital letters. Items in citations should be separated by commas. Page numbers should be included whenever applicable.

    Examples:

    1. *References to Journal Articles and Proceedings*

        Spillers,W.R. and Lefeochilos, E., "*Geometric Optimization Using Simple Code Representation*", Journal of the Structural Division, ASCE, vol. 106, no. ST5, 1980, pp. 959-971.

    2. *References to Books and Reports*

        Korsch, H.L. and Jodl, H. –J., "*Chaos: A Program Collection for the PC*", Springer-Verlag, 1994.

12. ***Units***: *SI* units must be used.

13. ***Conclusions***: A set of conclusions must be included at the end of the paper.

14. ***Submission of Paper***: Any paper submitted for publication in ZEDE must not have been published previously, or submitted for publication elsewhere; and if accepted for publication by ZEDE, the author/s shall transfer the copy right to ZEDE.

SILVER RECOVERY FROM WASTE X-RAY PHOTOGRAPHIC FILMS COLLECTED FROM HOSPITALS IN ADDIS ABABA

Mekurialem Demelash Erku[1], Anuradha Jabasingh S [1,*], Abubeker Yimam[1]
[1]Process Engineering Division, School of Chemical and Bio Engineering, Addis Ababa Institute of Technology, Addis Ababa University, Ethiopia
*Corresponding author's E-mail: anu3480@gmail.com

ABSTRACT

The present research reports a simple and efficient method for silver recovery using sodium hydroxide and sodium sulfide from the waste x-ray film. Response surface methodology was used to evaluate the effect of process parameters. The yield of silver by adopting this method was 1.07% at a stripping temperature of 70.88°C, at 10.97 min and NaOH concentration of 1.5M. The composition of recovered silver was determined by X-Ray Fluorescence (XRF).

Keywords: Photographic film, sodium hydroxide, XRF, Silver recovery

INTRODUCTION

Silver is rare, but occurs naturally in the environment. Ores of silver are argentite, chlorargyrite, and pyrargyrite [1]. The most common oxidation state of silver are +1, +2, +3 and +4 for $AgNO_3$, AgF_2, AgF_4 and K_2AgF_6 respectively [2]. Naturally occurring silver is composed of two stable isotopes, ^{107}Ag and ^{109}Ag, of which the former is more abundant [3,4]. Silver has more renowned applications. One of its most significant application is in the photographic industry. With the highest thermal conductivity and highest optical reflectivity it is found in abundance in the waste X-Ray photographic films [5]. Research claim that silver-containing wastes like used X-ray photographic film are toxic and considered as hazardous wastes [6]. In large doses, silver and compounds containing it lead to argyria, which results in a blue-grayish pigmentation of the skin, eyes, and mucous membranes [7]. Most households dispose these wastes into land and water bodies. The recoverable silver in the x-ray films are mostly present in the 'fix' and the 'bleach-fix' solutions. Most photographic and X-ray wastes contain silver thiosulfate with silver at a concentration of 5 parts per million (ppm). They are found in the fixer solution, rinse water, water baths and cleaning developer tank solutions [8].

Several technologies exist to recover silver from X-ray photographic film such as burning the film, electrolysis, metal replacement, bacterial, enzymatic methods and chemical precipitation. Except chemical methods, the other methods are expensive and time consuming to recover the silver [9]. The use of chemicals, sodium cyanide, nitric acid organic compounds cause environmental problems, whereas the decomposition by microorganism is slow [10]. Ion exchange processes, reduce the silver concentration in photographic effluent to levels in the range of 0.5 to 2 mg/L. Reverse osmosis (RO) and distillation recovery process are amongst the others used [11]. The present study explores the feasibility of high-purity silver recovery from waste x-ray films using sodium hydroxide with a focus on the optimization of the parameters that affect the process of silver recovery.

MATERIALS AND METHODS

Chemicals and reagents

Sodium hydroxide, NaOH; Sodium sulfide, Na_2S; Ethanol, C_2H_5OH, Hydrochloric acid, HCl; Borax decahydrate, $Na_2B_4O_7{\cdot}10H_2O$; Sodium carbonate, Na_2CO_3 was procured from Sigma-Aldrich, USA. The above listed chemicals were of Laboratory grade. Silicone oil was used in the oil bath. X-ray photographic films were collected from Black Lion medical faculty of Addis Ababa University, Ethiopia.

Processing the films

The collected x- ray photographic films were washed with distilled water and wiped with ethanol. These films were cut into 1 cm pieces and dried at 40°C for 30 min. NaOH at

various concentrations (0.5M, 1.5M and 2.5M) were prepared to strip the gelatin-silver layer from the base of the film.Na_2S was prepared to precipitate the silver from the stripped solution. HCl (11.65M) was prepared to validate the completion of stripping and presence of silver in the solution. An equal mixture of Borax (5g/dL) and sodium carbonate(anhydrous) was prepared for the processing[9].

Silver recovery

Twenty pieces (25 cm × 29 cm) for each run of prepared films were measured, cut, weighed and treated with 0.5M, 1.5M and 2.5 M NaOH in a 3L container placed in a silicone oil bath. The temperature was (50, 70 and 90°C) varied at three levels. The experiments were carried out by fixing the time (1, 10.5 and 20 min) at three levels. After the stripping process, the residual solution containing the colloidal black metallic silver was mixed with a proportionate amount of Na_2S to NaOH in the ratio (1:2). Stirring the solution resulted in the precipitation of the silver as a black sludge due to the common ion effect [11,12]. This was followed by decantation and filtration.

The black sludge was washed and dried in a muffle furnace at 500 °C for 30min. Equal amounts of $Na_2B_4O_7{\cdot}10H_2O$ and Na_2CO_3, was mixed with the dry black sludge in a ratio of 2:1 and the mixture was placed in the graphite crucible and heated for 90 min at 950°C. The molten pure silver was collected in a mould and its purity was measured by XFS using EDXRF Spectrometer (Sky Ray Model: EDX2800) at the Ethiopian geological survey, Addis Ababa. The process adopted for the recovery of silver is given in Fig. 1.

Process variables and optimization

Response surface methodology using Design Expert Software (version 9.0.0) was used to evaluate the effect of several process parameters and their interactions on the response variable [13]. The effects of the NaOH concentration, temperature and time of the stripping operation on the yield of silver recovered and its purity were studied.

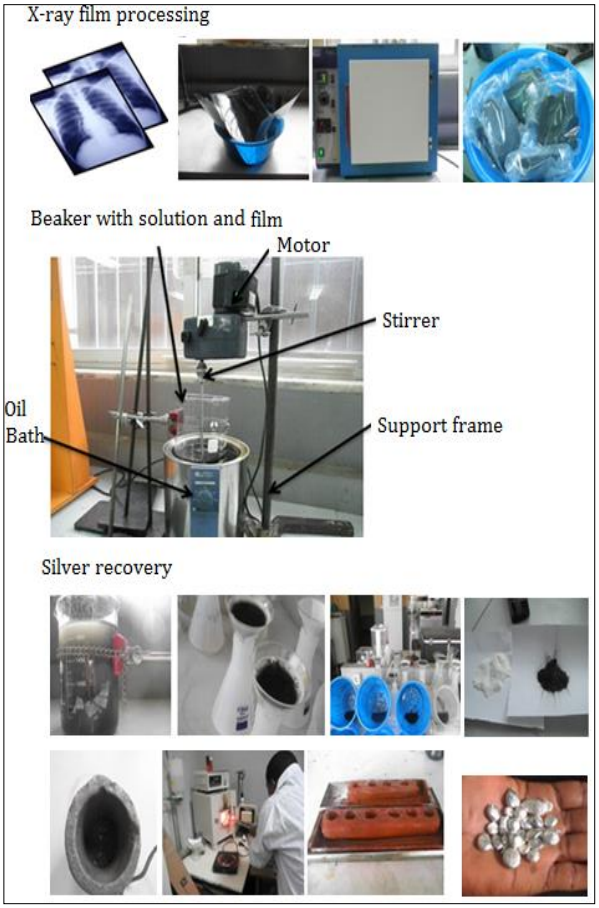

Fig. 1. Silver recovery from X-Ray films

The three factors were analyzed against three levels, the 3^3 design. 27 runs were performed to study the interaction among the factors and their effect on the amount of silver recovered using the response surface methodology. All the experimental sequences were performed in triplicate. The coded values of independent variables were found from equation (1)

$$x_i = \frac{X_i - X_0}{\Delta X},\ \text{i=1,2,3,...,k} \qquad (1)$$

where x_i is the dimensionless value of an independent variable, X_i is the real value of an independent variable, X_0 is the value of X_i at the center point and ΔX is the step change[13]. A second-order quadratic model was used to fit the quadratic equation

$$Y = \beta_0 + \beta_1 x_1 + \beta_2 x_2 + \beta_3 x_3 + \beta_4 x_4 + \beta_5 x_1^2 + \beta_6 x_2^2 + \beta_7 x_3^2 + \beta_8 x_4^2 + \beta_9 x_1 x_2 + \beta_{10} x_1 x_3 + \beta_{11} x_1 x_4 + \beta_{12} x_2 x_3 + \beta_{13} x_2 x_4 + \beta_{14} x_3 x_4 \qquad (2)$$

where Y is the measured response (silver recovery), x_1, x_2, x_3, x_4 are the coded independent input variables, β_0 is the intercept term, β_1, β_2, β_3, β_4 are the linear coefficients showing the linear effects, β_5, β_6, β_7, β_8 are the quadratic coefficients showing the squared effects and β_9, β_{10}, β_{11}, β_{12}, β_{13}, β_{14} are the cross product coefficients showing the interaction effects[14]. The optimum values of the factors were obtained by solving the regression equation, analyzing the surface of the three-dimensional response surface plot and also by the setting up of constraints for the levels of the variables [15].

RESULTS AND DISCUSSION

Yield of silver

The recovered silver yield was calculated as follows for each run and recorded (Table 1)

$$\%\ \text{yield} = \frac{(\text{weight of pure silver})}{(\text{weight of prepared film})} * 100 \quad (2)$$

During the measurement of the yield, the weight of used x-ray film is taken as input and the amount of pure silver recovered is used as output.

There was a considerable variation in the amount of silver recovered irrespective of the size and type of the x-ray film. This fact is due to the dependency of the area covered by the x-ray image on the surface of the entire film. The data has been randomized during Design expert software (Table 2).

Table 1. Factors and corresponding levels

Factors	Range	Levels		
		-1	0	+1
A: Conc. (Mol/L)	0.5-2.5	0.5	1.5	2.5
B:Time (min)	1 - 2 0	1	10.5	20
C: Temp. (°C)	50-90	50	70	90

Effects of process parameters

The yield of silver was determined at each combination of the process settings. NaOH concentration emerged to be the most important factor during stripping and recovery of silver. Stripping of silver from the film base was favorable at short stripping time at high NaOH concentration [16].

But increasing NaOH concentration beyond 1.5 M resulted in a difficulty of silver recovery due to precipitation. Fig.2a -Fig.2c shows that the concentration of sodium hydroxide had a large impact on the yield of silver. Increasing NaOH concentration until 1.5M increases the yield rapidly, but further increasing the concentration decreases the yield by the same rate.The silver yield was observed to increase slightly as there was an increase in the stripping time until 15 min. The contact between the reagent and film base was the key factor responsible for the stripping away of the silver from the film base. Temperature has a significant effect on the yields of the silver. Increasing the temperature until 70°C, increases the yields of silver. Increasing temperatures above 70 °C decrease the yield due to the interaction effects of the factors. The temperature is the most important factor to make the silver more exposed to stripping. Very high temperatures are not suitable for the silver stripping, due to the disintegration of stacked gluten employed in the manufacture of x-ray films. The 3-D response surfaces were plotted to understand the interaction between the variables and to determine the optimum levels of each variable for maximum response (Fig.3a-Fig.3c). 3D surfaces show the interaction effects of concentration and time with respect to the yield of silver. The interaction plots show the increasing yield of silver until 15 min at 1.5M NaOH concentration and yield was found to decrease after this treatment time. Higher stripping time, favor complete stripping of silver from the film into the stripping solution. Longer times of exposure resulted in the suspension of silver rather than it settling, making the subsequent decantation and separation processes difficult and also resulting in degradation. Higher yields of silver are obtained at 1.5M NaOH and 70° C. All the three factors were significant as found from the ANOVA results. All the factors had values of "prob> F" less than 0.05, thus proving the significance of the results (Table 3).

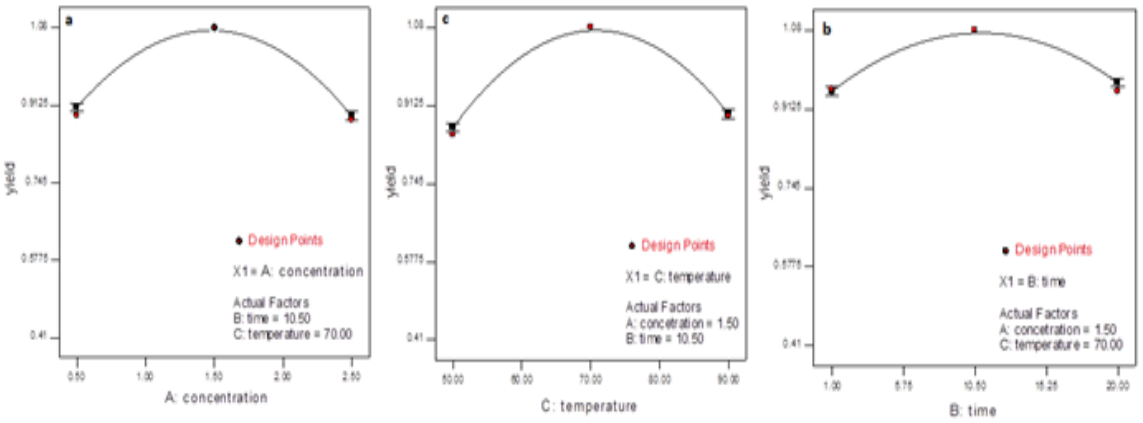

Fig. 2. (a) Effect of NaOH concentration (b) Effect of time (c) Effect of temperature.

Table 2. Factors and responses

Run No	Factors			Film Weight(g)	Pure Silver Weight(g)	Yield(%)
	A	B	C			
1	0.50	1.00	50.00	354.70± 0.46	1.45± 0.08	0.41±0.02
2	0.50	10.50	50.00	354.10± 1.15	2.16± 0.32	0.61±0.06
3	0.50	20.00	50.00	353.20± 0.36	2.15± 0.27	0.61 ±0.04
4	0.50	1.00	70.00	345.37± 0.55	2.56± 0.70	0.74 ±0.02
5	0.50	10.50	70.00	347.50± 0.79	3.09± 0.09	0.89 ±0.03
6	0.50	20.00	70.00	352.60± 2.34	3.07± 0.35	0.87 ±0.03
7	0.50	1.00	90.00	353.70± 0.46	2.30± 0.28	0.65 ±0.06
8	0.50	10.50	90.00	351.40 ± 1.65	2.85± 0.29	0.81 ±0.04
9	0.50	20.00	90.00	354.20± 1.31	2.55± 0.34	0.72 ±0.04
10	1.50	1.00	50.00	352.00± 1.41	2.50± 0.51	0.71 ±0.02
11	1.50	10.50	50.00	348.70± 0.10	2.96± 0.40	0.85 ±0.04
12	1.50	20.00	50.00	353.80± 0.26	2.76± 0.13	0.78 ±0.07
13	1.50	1.00	70.00	348.80± 0.72	3.31± 0.49	0.95 ±0.04
14	1.50	10.50	70.00	358.10± 0.36	3.87± 0.08	1.08±0.01
15	1.50	20.00	70.00	347.60± 1.08	3.30± 0.29	0.95±0.06
16	1.50	1.00	90.00	355.50± 0.79	2.81± 0.16	0.79 ±0.04
17	1.50	10.50	90.00	353.90± 0.20	3.15± 0.27	0.89 ±0.08
18	1.50	20.00	90.00	348.20± 0.26	2.71± 0.15	0.78 ±0.04
19	2.50	1.00	50.00	355.80± 0.95	2.46± 0.04	0.69 ±0.02
20	2.50	10.50	50.00	352.10± 0.62	2.75± 0.16	0.78 ±0.02
21	2.50	20.00	50.00	349.70± 2.04	2.13± 0.25	0.61±0.05
22	2.50	1.00	70.00	347.70± 0.35	2.78± 0.21	0.80 ±0.04
23	2.50	10.50	70.00	358.60± 0.80	3.14± 0.38	0.88 ±0.03
24	2.50	20.00	70.00	350.30± 0.75	2.52± 0.24	0.72 ±0.07
25	2.50	1.00	90.00	350.40± 0.95	2.06± 0.34	0.59 ±0.09
26	2.50	10.50	90.00	349.70± 0.85	2.20± 0.23	0.63 ±0.02
27	2.50	20.00	90.00	354.90± 0.96	1.60± 0.32	0.45 ±0.01

Table 3. Analysis of Variance for Silver Yield

Source	Sum of Square	df	Mean Square	F value	p-value Prob > F
Model	1.06	9	0.12	603.68	< 0.0001
A	0.0015	1	0.0015	7.78	0.0107
B	0.0016	1	0.0016	8.35	0.0085
C	0.0039	1	0.0039	20.06	0.0002
AB	0.041	1	0.041	212.97	< 0.0001
AC	0.076	1	0.076	390.79	< 0.0001
BC	0.0059	1	0.0059	30.09	< 0.0001
A^2	0.22	1	0.22	1130.04	< 0.0001
B^2	0.094	1	0.094	483.15	< 0.0001
C^2	0.27	1	0.27	1378.80	< 0.0001
Residual	0.0043	22	0.0002		
Lack of Fit	0.0043	17	0.0003		
Pure Error	0.000	5	0.000		
Cor Total	1.06	31			

There is only a 0.01% chance that a "Model The Model F-value of 603.68 implies the model is significant F-Value" this large could occur due to noise. Values of "Prob > F" less than 0.0500 indicate model terms are significant. In this case A, B, C, AB, AC, BC, A^2, B^2, C^2 are significant model terms. Values greater than 0.1 indicate the model terms are not significant[14]. If there are many insignificant model terms (not counting those required to support hierarchy), model reduction may improve your model.

The "Pred R-Squared" of 0.9899 is in reasonable agreement with the "Adj R-Squared" of 0.9943. "Adeq Precision" measures the signal to noise ratio [15]. A ratio greater than 4 is desirable. The ratio of 84.527 indicates an adequate signal. This model can be used to navigate the design space. Based on the above significant factors, the coefficients for the model were estimated.The final equation in terms of coded factors is given as follows

$$Yield = 1.07 - 0.0092A + 0.0095B + 0.015C - 0.059AB - 0.080AC - 0.022BC - 0.18A^2 - 0.11B^2 - 0.19C^2$$

The positive coefficients were found to maximize the yield, whereas, the negative coefficients drastically minimized the recovery of silver. Thus, increasing the concentration had an inverse relationship with the silver yield.

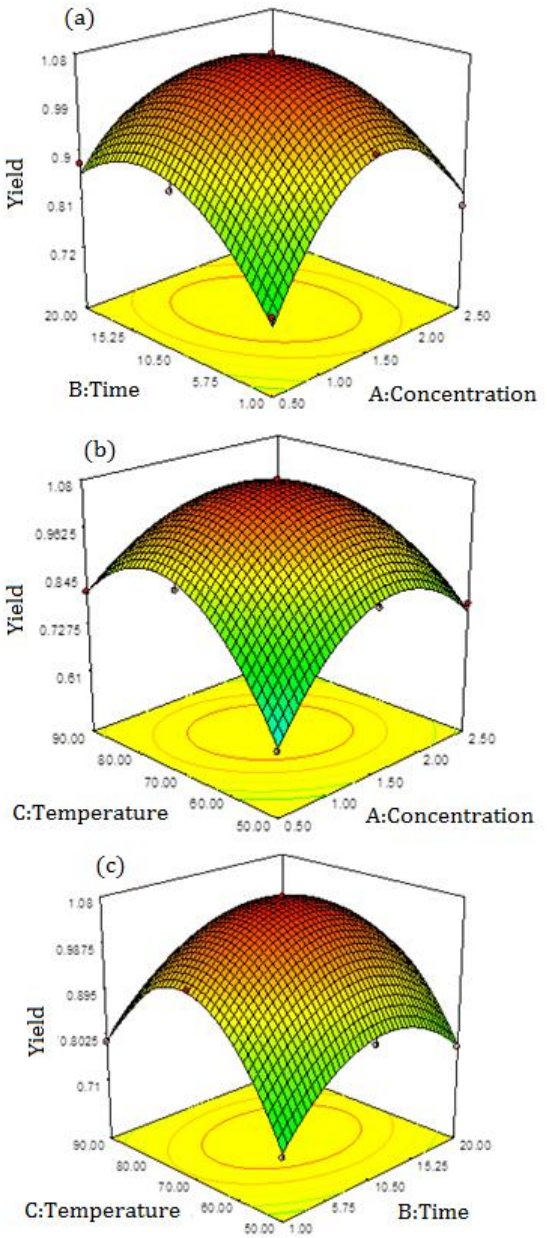

Fig. 3. (a) Effect of NaOH concentration and time (b) Effect of temperature and NaOH concentration (c) Effect of temperature and time.

However, the parameters including the time and temperature with positive coefficients had a direct proportionality with the yield. Increasing time would allow the silver stripped completely from the film base and high temperatures were found to activate and expose the silver to be leached out [12]. The interaction and square of these factors have inverse proportionality with the yield.

Parity plot was prepared to investigate the agreement between experimental (actual) values

and model predictions (Fig. 4). The actual values and the predicted values were compared. The actual value was the measured response data for the runs, y_i, and the predicted value was the value predicted from the model, generated by using the prediction equation.

There was a satisfactory agreement between experimental and predicted values. Optimization may be interpreted as the way to find those values of controllable independent variables that give the most desired value of the dependent variable. Numerical optimization was carried out considering each value of the response and the goal of silver recovery or yield is set to maximum. The optimum yield of silver was 1.07% at a NaOH concentration of 1.46 Mol/L, stripping time of 10.97 min and temperature of 70.88°C. At these optimum values, the average silver content of the waste x-ray film was 0.26 mg/cm^2. The average yield of the method was 54%, according to silver content based on the 0.26mg/cm^2, the average silver content of the waste x-ray film. The desirability output of the model was 0.992.

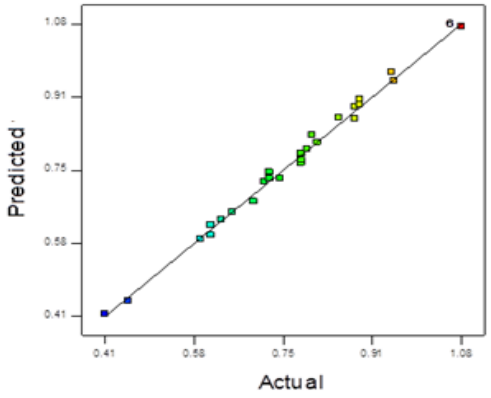

Fig. 4. Parity plot

Product characterization

The purity and the trace impurities present in the recovered silver were quantified and provided in Table 4. The X-Ray Fluorescence (XRF) machine sampled silver product of about 0.8 mm diameter and 15 mm depth (Fig 5).

Table 4. Composition of the recovered silver

Weight (g)	Cu %	Zn %	Ag %	Au %	Pd %	Cd %	Sn %
2.52	<0.01	0.3	98.28	<0.01	0.52	0.3	<0.01
1.61	<0.01	0.3	97.77	<0.01	0.52	0.3	0.54

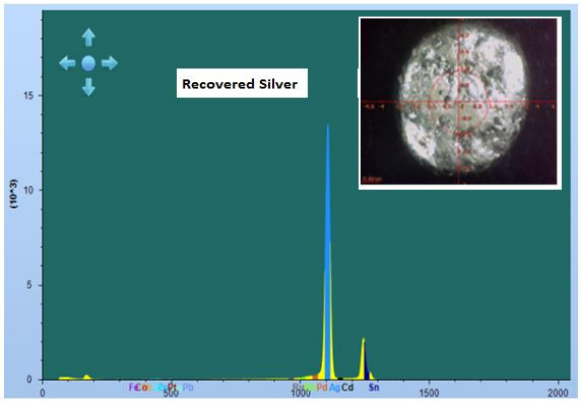

Fig. 5. Spectrum of recovered silver on XRF

The machine generated an average composition of the impurities in the samples. The Table 4 shows the purity of the first sample as 98.28 % and the second sample as 97.77% purity. The average purity remained 98.03 %, these results were encouraging as the impurities in the samples were less than 2%. Literatures supported an average purity of 99.24% [12]. Metals including Zn, Au, Pd were also detected during the testing processes.

CONCLUSIONS

The optimal recovery conditions of silver were stripping temperature of 70.88°C, stripping time of 10.97 min and NaOH concentration of 1.46 M. Under these conditions, the obtained silver had 1.07% yield and 54% recovery. The factors influencing the stripping process of silver were in the order of stripping temperature, stripping time and NaOH concentration. It is concluded that silver from used x-ray film had a purity of 98.28 %.

REFERENCES

[1] ATSDR., *"Toxicological profile for silver"*, Agency for Toxic Substances and Disease Registry U.S. Public Health Service, December 1990.

[2] **Riedel,** S., and **Kaupp,** M., "***The highest oxidation states of the transition metal elements",*** Coordination Chemistry Reviews 253 **(**5–6**), 2009,** 606-624**.**

[3] IUPAC., "*Atomic weights of the elements*", International Union for Pure and Applied Chemistry, Technical report, 2007.

[4] Bjelkhagen, H.I., "*Silver-halide recording materials: for holography and their processing*". Springer, 1995, 156-166.

[5] Masser, S.H., "*Method of recovering silver from waste photographic film and paper*", American patent, 4759914, 1988,CI 423-439.

[6] White, I.R., and Rycroft, R.J.G., "*Contact dermatitis from silver fulminate-fulminate itch"*. Contact Dermatitis, 8, 1982, 159-163.

[7] Samson, O.M., and Edison, M., "*Review of Silver Recovery Techniques from Radiographic Effluent and X-ray Film Waste*", Proceedings of the World Congress on Engineering and Computer Science, 2, 2014, San Francisco, USA.

[8] Kodak., "*Recovering silver from photographic processing solutions*", Publication no. J-215 Eastman Kodak Company, 1999.

[9] Rawat, J.P., and Iqbal, S., Kamoonpuri, M., "*Recovery of silver from laboratory wastes"*, Journal of Chemical Education, 1986, 63 (6), 537.

[10] He, J., and Kappler, A., "*Recovery of precious metals from waste streams*", Microbial Biotechnology, 10, 1194-1198, 2017.

[11] Goshima, T., Hori, K., Yamamoto, A., "*Recovery of silver from radiographic fixer*", Oral Surgery, Oral Medicine, Oral Pathology,77(6),1994, 684-688.

[12] Nikiboglu,N., Toscali, D., and Nisli, G., "*A novel silver recovery method from waste photographic films with NaOH stripping*". Turkish Journal of Chemistry 27, 2003, 127-133.

[13] Box, G.E.P., and Wilson, K.B., "*On the experimental attainment of optimum conditions*", J. R. Stat. Soc. Ser. B-Stat. Methodol.13, 1951, 1-45.

[14] Anuradha Jabasingh, S., Valli Nachiyar, C., "*Optimization of cellulase production by Aspergillus nidulans: application in the biosoftening of cotton fibers*", World Journal of Microbiology and Biotechnology, 27(1), 2011, 85-97.

[15] Anuradha Jabasingh, S, Valli Nachiyar, C., "*Utilization of pretreated bagasse for the sustainable bioproduction of cellulase by Aspergillus nidulans MTCC344 using Response surface methodology*", Industrial Crops and Products, 34(3), 2011,1564-1571.

Anuradha Jabasingh, S., "*Utilization of pretreated coir pith for the optimized bioproduction of cellulaseby Aspergillus nidulans*", International Biodeterioration and Biodegradation, 65 (1), 2011, 1150-1160.

STATISTICAL ANALYSIS OF PROPERTIES OF TIMBER SPECIES FOR STRUCTURAL USE

JIMOH, Abdullahi Alao[1] and AINA Samuel[2]
[1,2]Department of Civil Engineering, University of Ilorin, Ilorin, Nigeria
[1]Correspondence e-mail address: aajimoh4real@yahoo.com

ABSTRACT

This study investigated the physical and mechanical properties of two Nigerian timber species- Azadirachta indica and Xylopia aethiopica for structural use. Three logs of each species were obtained at different locations of the country, seasoned naturally and their structural strength properties were determined and converted to strength at moisture content of 18%. These logs were cut into specimens to facilitate the determination of the properties of the timber. A total of 45 specimens for each property, free from visible defects were used. Basic physical properties of the samples like moisture content, specific gravity and density were evaluated. Tensile strength, modulus of rupture, modulus of elasticity, compression, shear and hardness were the mechanical properties determined with specimen shapes prepared following BS 373 (1957) specifications and specimen tested using a Universal Testing Machine (UTM). Results were analysed statistically to evaluate the mean, standard deviation, statistical significant difference and confidence limits. Using these statistical results and based on BS 5268-2 (2002), Azadirachta indica and Xylopia aethiopica species were characterized and fell into strength classes D30 and D70, respectively.

Keywords:Azadirachta, indica, Xylopia aethiopica, Properties

INTRODUCTION

Timber is a complex building material owing to its heterogeneity and species diversity. Timber does not have consistent, predictable, reproducible and uniform properties as the properties vary with species, age, soil and environmental conditions [1]. The need for local content in construction of engineering infrastructure is now a serious challenge. This is because vast quantities of local raw materials which must be processed and used for cost effective construction abound. Construction activities based on these locally available raw materials are major steps towards industrialization and economic independence for developing countries. This explains huge interest and considerable intellectual resources being invested in understanding the mechanical or structural properties of the Nigerian timber [2].

The primary goal of engineered construction is to produce a structure that optimally combines safety, economy, functionality and aesthetics. Timber, like other building materials, has inherent advantages that make it especially attractive in specific applications [3]. Structural timber is the timber used in framing and loadbearing structures, where strength is the major factor in its selection and use. The main issue is to find design methods ensuring that the relevant performance criteria are met with a certain desired level of confidence That means that the risk of non-performance should be sufficiently low.

The main challenge in design with timber as structural member is to be acquainted with sufficient data about a given species of the timber to ensure that the relevant performance criteria are met, as specified in relevant standards and codes. This implies that failure risk is reduced to the extent to which structural information about a given species of timber is readily available to timber designers, specifiers and construction regulators. A significant element of uncertainty is associated with lack of information on the physical variability as well as structural behavior of material under load, [4]. The question of strength characteristic of these timber species is therefore aimed at reducing the structural risk of using them for supporting and sustaining loads in structural systems.

Azadirachta indica, is of the mahogany family Maliaceae*;* popularly known as neem tree or dogonyaro (Hausa). It is an evergreen tree. Neem is native to east India and Burma and grows much in South East Asia (SEA) and West Africa and it is cultivated in Pakistan, Peninsular Malaysia, Singapore, Philippines, Australia. Plantation of Neem in small scale in Europe and United States of America has shown success [5]. It has been in use since ancient times to treat a number of human ailments and also as household pesticide [6, 7,8,9,10] . Neem tree is about 12-18 metres in height with a circumference ranging between 1.8 and 2.4 metres. Neem is a flowering plant which will produce flower on 3-5 years of age [11] in which the flowers are 4-7mm in length and 6-10mm in width [12]. The flower has a jasmine like odour and white in colour. The leaves are dark green in colour up to 30 cm in length [11] and has 3 lobed stigmata and seeded drupes [13] . The fruit of Neem is about 2cm long with white kernels and when mature it is able to produce 50kg of fruit yearly [11]. The branch of Neem is dense with up to 10cm in length and has a dark brown bark [12]. Furthermore, Neem tree is able to adapt to very dry condition [11, 12] which is up to 120°C with minimal rainfall of 18 25 mm per year [5]. Besides that, the plant can grow well in calcareous soil with the pH up to 8.5 [14]. *Xylopia aethiopica* commonly known as "African guinea pepper" or "Ethiopian pepper" is wide spread in tropical Africa, Zambia, Mozambique and Angola. In Nigeria, it is found all over the lowland rain forest and most fringe forest in the Savanna zones of Nigeria [15] .

X. *aethiopica* is a member of the family Annonaceae, it is a tree of more than 20 m of height and 60 to 75 cm in diameter. It grows in the forest zone and especially along the rivers and in arid areas. The fruit is a slightly hooked cylindrical pod reaching 2 to 3 mm in width. The mature fruits of green colour take a brown -black colouration after drying and they are commonly used as spices [16 , 17]. The leaves simple, alternate, oblong, elliptic to ovate, 8-16.5 by 2.8-6.5 cm, leathery, bluish-green and without hairs above, but with fine brownish hairs below, margin entire, and glabrous; petiole 0.3-0.6 cm, thickset and dark-coloured. Flowers are bisexual, solitary or in 3-5 flowered fasicles or in strange, sinuous, branched spikes, or cymes, up to 5.5 by 0.4 cm and creamy-green. The fruits are small, carpels 7-24, forming dense cluster, twisted bean-like pods, dark brown, cylindrical, 1.5-6 cm long and 4-7 mm thick; the contours of the seeds are visible from outside. Seeds are black, 5-8 per pod, kidney-shaped seeds of approximately 10 mm length with a yellow papery aril. The hull is aromatic, but not the seed itself [18].

John-Dewole et al. [19] reported the medicinal uses of the fruit extract of *X.aethiopica* in the treatment of bronchitis, oedema, dysentery and febrile pains. In Congo, the infusion of the extract of the bark of the tree into palm wine is used in the treatment of asthmatic attack, stomach aches and rheumatism at dosage rate of one or two glasses per day [20]. In Senegal, the dried root crushed into powder is used as mouthwash for toothache and pyorrhoea. In Cote D'ivoire, the fruits are recommended as a source of blood tonic to women, after baby delivery, for blood replenishment. It is used as antihelminthic and also as analgesic for chest pain [21]. *X.aethiopica* is used locally in Nigeria for the treatment of cancer and ulcers. The powdered bark of the tree is dusted onto ulcerous wounds, while a decoction of the leaves and roots is a general tonic for fever in Nigeria [22] . The crude extract exhibit a strong anti-feedant activity on subterranean termite, Reticulitermes speratus [19].

Stress grading is the process of assigning timber specie to a predefined strength/stress class or grade provided in available codes of practice. Strength class is the classification of timber based on particular values of grade stress, modulus of elasticity and density in reference [23] . Over the years, stress grading has usually been done in two ways;

(i) Visual grading: This method sorts timber into grades on the attributes of visual characteristics i.e. knots, pith, sloping grain.

(ii) Machine grading: This assigns stress grade to timber according to its stiffness. The grade is assigned by slotting the minimum local stiffness into thresholds ranges. The thresholds are selected so that populations of the timber meet or exceed characteristic strength and stiffness for the grade.

This means that machine-graded timber will generally have a higher stiffness for a given strength than will visually graded timber of the

same species. In practice, it is the stiffness property (Modulus of Elasticity or MOE or Young's Modulus), that is limiting in the design of most timber structures for everyday use. Hence machine grading is the more relevant grading method. In 2015, Ataguba *et al*.,[24] did a comparative study of the mechanical properties of *Gmelina Arborea*, *Parkia Biglobosa* and *Prosopis Africana* timbers for structural use and concluded that the three species proved to have physical and mechanical properties that make them suitable for structural engineering use as hardwoods by grading them into strength classes between D30 – D70 when compared with Table 8 of BS 5268. It was part of his recommendation that tree species like Neem tree should be characterized for structural use.

Zziwa *et al*., [26] characterized timbers for building construction in Uganda. Seventeen timber species were characterized according to the relevant Ugandan code of practice. After the study, four strength groups namely SG4, SG8, SG12 and SG16 were derived in view of the anticipated loading categories in building construction. It is on this back-drop that this study aim at characterising A. Indica and X. Aethiopica by examining their physical and mechanical properties.

MATERIALS AND METHODS

Three stems of each timber species were gotten from different areas of Nigeria and transported to a sawmill for processing. The tree stems were 3.8m to 4.1m long and varied from 0.32m to 0.39m in diameter.

The stems were sawn into commercial sizes and seasoned in open air to equilibrium moisture content with the environment. Samples were taken along the stem and marked top, middle and bottom as shown in Figure 1. It was ensured that the selected timber was free of defects and was as straight as possible.

Specimens were cut from the stem for the physical properties (moisture content, specific gravity and density) and mechanical properties (tensile strength, modulus of rupture, and modulus of elasticity, compression, shear and hardness).

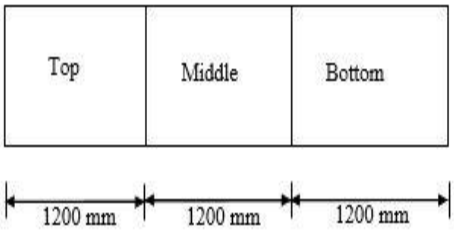

Figure 1 Schematic diagram of Sample stem Preparation

There were 18 test specimens for each physical property test (6 samples each from the top, middle and bottom position). Forty-five (45) specimens were used for each mechanical test (15 samples for each top, middle and bottom portions). The specimens were prepared in accordance with BS 373:1957 [27] (Methods of testing small clear specimens of timber). The code recommended 2cm standard size of testing small clear specimens. The test was done using a Universal Testing Machine (UTM) of capacity 100kN at National Centre for Agricultural Mechanization (NCAM) in Ilorin town, Nigeria.

The requirement is that the physio-mechanical properties of wood should be determined at the moisture content of 12% as standard. The equation relating the failure strength at a moisture content of test to the strength at the standard moisture content of 12%, is given by

$$F_{12} = F_w(1 + \alpha(W - 12) \qquad (1)$$

where F_{12} is the failure stress at 12% moisture content, W is the moisture content at the time of testing, F_w is the failure stress at the moisture content at the time of testing, α is a correction factor given in Table 1. The reduction formula is valid for moisture content of 8% to 23%.

Table 1: Correction Factor, αState of stress	α (for all wood species)
Compression parallel to the grain	0.05
Static bending	0.04
Shearing stress parallel to the grain	0.03

Source: Wooden and Plastic Structures by Karlsen G. and Slitskouhov Yu [28]. Equation (1) converts the failure stress of the mechanical properties at the existing moisture content to values at moisture content of 12% . The computed stress values were thereafter converted to their respective values at moisture content of 18% using Equation. (2) (this is the

acceptable moisture content of timber to be used in Northern Nigeria). From these stresses, the basic stress were computed using expressions in Table 2.

Stress at 18% moisture content = $\frac{F_{12}\text{x}18}{12}$ (2)

Where F_{12} = failure stress at 12% moisture content.

Eighty percent (80%) grade stress of the timbers was calculated as well as 95% and 99% confidence limits of the failure stress. Analysis of Variance (ANOVA) was used to determine if there is significance difference between the properties of the top middle and bottom positions of the timber species.

Basic stresses

These are given by [29] as summarized in Table2

Table 2 Basic stress expressions

Basic stress	Expression for basic stress	Definition of terms
bending stress parallel to the grain	$f_{b\,par} = \frac{f_m - 2.33\sigma}{2.25}$	f_m = mean value of the failure stresses σ = standard deviation of the failure stresses
basic tensile stresses parallel to the grain	$t_{b\,par} = \frac{f_m - 2.33\sigma}{2.25}$	As above
basic compressive stresses parallel to grain	$c_{b\,par} = \frac{f_m - 2.33\sigma}{1.4}$	As above
basic compressive stresses perpendicular to the grain	$c_{b\,per} = \frac{f_m - 1.96\sigma}{1.2}$	As above
basic shear stresses parallel to the grain	$v_{b\,par} = \frac{f_m - 2.33\sigma}{2.25}$	As above
relationship between the E_{mean} and the statistical minimum value of E appropriate to the number of species acting together	$E_N = E_{mean} - \frac{2.33\sigma}{\sqrt{N}}$	E_N is the statistical minimum value of E appropriate to the number of pieces N acting together (N=1, E_N becomes the value for E_{min}) and σ is the standard deviation.

RESULTS AND DISCUSSION

Tables 3 and 4 show the results obtained from the laboratory for the physical and mechanical properties of the timbers as well as the 80% grade stress with 95% and 99% confidence limits of the failure stress. Likewise, the results of the ANOVA statistical test are presented in Tables 5 and 6 while Figures 2 and 3 show the typical Stress-Strain curves for the timber species.

Comparison of results

Comparison of the two timber strength is as follow. *Xylopia aethiopica* has higher values of MOR, compressive strength parallel to grain, tensile strength parallel to grain, radial and tangential hardness as well as shear strength than *Azadirachta indica*. The differences in strength may be due to the differences in density.

The mean relative density of aethiopica is 1.15 whereas that of indica is 0.83. Mechanical property of timber is reported to increase with increase in density [1]. However, with the lower density of *Azadirachta indica* it has higher mean compressive strength perpendicular to grain, which may suggest that this property is not density related.

Comparison of each timber properties indicate that *Azadirachta indica* mean compression strength parallel to grains is comparable to its mean strength perpendicular to the grains, whereas for *Xylopia aethiopica*, its compressive

strength parallel to grain is three times higher than the strength in compression perpendicular to grain. This suggests that there is no definite pattern and similar way of behaviours in material properties. A high degree of variability in property has been demonstrated by these timber [1] . For example Compression strengths parallel to the grains ranged between 15.93 N/mm^2 and 22.04 N/mm^2 with standard deviation of 2.58 while the compression strengths perpendicular to the grains ranged between 15.18 N/mm^2 to 26.09 N/mm^2, with standard deviation of 4.26.

Similarly, *Azadirachta indica* performed better in shear (mean result is 7.27) than in tension of mean value 5.53 N/mm^2 while it is opposite for *Xylopia aethiopica* with mean tensile strength of 73.55 N/mm^2 than in shear of 12.3 N/mm^2. All these are as a result of variability in timber caused by its natural occurrence which is uncontrollable. Comparison of the two timbers with other timber especially the Greenheart reported as very strong [30] is as follow. Greenheart density is 977 kg/m^3 which shows a similar value with that of Negro Pepper (*Xylopia aethiopica)* but higher than for Neem timber. The modulus of rupture for Greenheart is 181 N/mm^2 [30] , which is 10 times that of Neem timber (19.04 N/mm^2) obtained in this study, but about 2 times that of Negro Pepper (80.36 N/mm^2). A timber that is in the same strength range with Negro Pepper is Gossweilerodendron balsamiferum Harms, popularly called Agba. Agba bending strength is 81 N/mm^2 , similar to 80.36 N/mm^2 obtained for Negro Pepper in this study.

Classification of timber

In classification, the values of modulus of elasticity (MOE) and the static bending strengths also show that the timber types are hardwood of higher strength classes (between strength classes D30 and D70) when compared with the standard values for strength grades in Table 8 of BS 5268 [23]. The densities obtained ranged from 740 to 1160 kg/m^3 also show that the timbers investigated belong to class of heavy timbers since values obtained are greater than minimum value 720 kg/m^3 specified for heavy timber class [31]. Basic stress given in Table 4 can be used in classification of the two timber species according to NCP 2 (1973) where classes are from the strongest N_1 to weakest N_7. While basic stress for Neem timber falls below the N_7 group, Negro Pepper fall into N_2 . In this group (N_2), basic stresses are : Bending and tension parallel to grain 28.0 N/mm^2,compression parallel to grain 22.4 N/mm^2, shear parallel to grain 3.55 N/mm^2 compression perpendicular to grain 5.0 N/mm^2 and mean value modulus of elasticity 12500 N/mm^2, which agree with the values in Table 4 for Negro pepper.

Statistical analysis

The variation in mechanical strength results are given in Table 3. In order to reduce failures as a result of the variations, results for confidence limits at 95 and 99 % are in some cases recommended in designs [1]. Therefore its computation is carried out and results are given in Table 4. Also the Basic strength results are also recommended [30]. It is obtained by dividing the confidence limits results by some factors. The grade stress is obtained by applying a factor of 0.8 (=80 %) to basic stress in order to take care of defects during application.

Analysis of variance (ANOVA)

Analysis of variance is carried out using the Null hypothesis that there is no significant different between the mean results and that of the population. Critical significance level α of 5 % was set. The null hypothesis is rejected if $P \leq \alpha$, that is, there is significant difference; or accepted if $P > \alpha$, that is, there is no significant difference. ANOVA results are shown in Tables 5. While some results show some significant difference some do not show the significant difference.

For *Azadirachta indica*, , P = 0.05 for compressive strength parallel to the grain, meaning that there is significant difference between the top, middle and bottom position. Similarly there is significant difference for compressive strength perpendicular to the grain (P = 0.034), tensile strength parallel to the grain (P = 0.001), radial hardness (P = 0.022). However, there were no significant difference in its MOR (P = 0.13), tangential hardness (P = 0.925), and shear strength parallel to the grain (P = 0.215). On the other hand, *Xylopia aethiopica* showed a significant difference between the top, middle and bottom position in its tensile strength parallel to the grain (P = 0.00), while there were no difference in its MOR (P = 0.393), compressive strength parallel to the grain (P = 0.403), compressive strength

perpendicular to the grain (P = 0.524), radial hardness (P = 0.051), tangential hardness (P = 0.115), and shear strength parallel to the grain (P = 0.369). The level or intensity of the significant differences is demonstrated by the respective different F values as shown in the table.

Stress-strain curve

The typical stress-strain curve in Figure 2 is for Neem timber. Values of stress and strain are obtained automatically as print out after each test from the computer attachment to the testing machine. The computer uses the input values of cross sectional areas to divide the experimental load on the specimens to obtain stress results and similarly, the initial length values input are used to divide the elongations of the specimen to obtain the strain values.

The curve in Figure 2 shows that for Neem timber, the yield point is around 6 N/mm^2 , while the ultimate stress is about 9.4 N/mm^2. At these two points the strains are 0.005 mm/mm and 0,02 mm/mm respectively. However, an arbitrary strain value of 0.05 mm/mm is taken as the dividing line between the brittle and ductile classes of materials [32,33]. The timber experimental strain values are less than the 0.05 , thus showing that the Neem timber is a brittle material. Also Figure 3 shows the stress strain curve for Negro Pepper timber. In this case the yield stress is around 35 N/mm^2 while the ultimate stress is 75 N/mm^2.

The strain values at these two points are 0.004 mm/mm and 0.013 mm/mm , respectively. These values show also that Negro Pepper timber belongs also to brittle materials. Using the timber species yield stress values and divide them by their respective strains, it gives the moduli of elasticity as 1200 N/mm^2 and 8750 N/mm^2 for Neem and Negro Pepper respectively.

That of Negro Pepper is about 7 times value for Neem timber. However, steel material possesses the modulus of elasticity of 200,000 N/mm^2 , about 167 times that of Neem timber and 23 times that of Negro Pepper. Greenheart timber modulus of elasticity is 21000 N/mm^2, about 1.4 times of Negro timber. Agba has modulus of elasticity of 7600 N/mm^2 about 0.87 that of Negro Pepper timber..

Table 3 Physical and mechanical properties test results

Timber Name	Statistical parameters	Moisture content (%)	Density (g/cm^3)	Specific gravity	Bending stress (N/mm^2)	Compressive stress parallel to grain (N/mm^2)	Compressive stress perpendicular to grain (N/mm^2)	Tensile stress (N/mm^2)	Radial Hardness (N)	Tangential Hardness (N)	Shear stress (N/mm^2)	Modulus of Elasticity (N/mm^2)
Neem Tree *(Azadirachta indica)*	Min.	10.87	0.74	0.79	5.66	15.93	15.18	3.02	418.42	399.28	3.74	2737
	Max.	15.67	0.90	0.94	44.58	22.04	26.09	9.26	546.67	544.09	11.28	5950
	Mean	12.59	0.83	0.88	19.04	19.38	19.65	5.53	478.28	468.92	7.27	4239
	SD	1.99	0.07	0.06	3.67	2.58	4.26	2.62	53.48	57.74	3.07	1367
Negro Pepper (*Xylopia aethiopica)*	Min.	10.4	0.79	0.99	43.99	39.7	11.92	71.87	606.63	620.09	7.75	6293
	Max.	21.91	1.16	1.20	131.92	67.7	17.56	74.55	764.52	786.24	17.45	14461
	Mean	16.7	1.15	1.09	80.36	53.52	14.56	73.55	704.84	684.91	12.3	10060
	SD	4.71	0.17	0.09	15.53	14.69	2.99	1.46	88.38	89.09	5.71	4278

Table 4: Failure stress, basic stress and grade stress at 18% moisture content

Timber Name	Observed values	Bending stress (N/mm^2)	Compressive stress parallel to grain (N/mm^2)	Compressive stress perpendicular to grain (N/mm^2)	Tensile stress (N/mm^2)	Shear stress (N/mm^2)	Modulus of Elasticity (N/mm^2)
Neem Tree *(Azadirachta indica)*	Failure stress	28.56	29.07	29.48	8.3	10.91	6258
	95% Confidence limit	17.2, 20.14	18.6, 20.16	18.37, 20.93	4.74, 6.32	6.35, 8.89	3828, 4649
	99% Confidence limit	17.57, 20.51	18.34, 20.42	17.94, 21.36	4.48, 6.58	6.04, 8.5	3690, 4787
	Basic stress	8.89	16.47	17.6	0.97	2.68	5296
	80% Grade stress	7.11	13.18	14.08	0.78	2.14	4237
Negro Pepper Tree *(Xylopia aethiopica)*	Failure stress	120.54	80.28	21.84	110.33	18.45	15089
	95% Confidence limit	75.69, 85.03	49.11, 57.93	13.66, 15.46	73.12, 73.99	10.59, 14.01	8774, 11345
	99% Confidence limit	74.13, 86.59	47.62, 59.42	13.36, 15.76	72.97, 74.14	10.01, 14.59	8343, 11776
	Basic stress	37.49	32.89	13.32	47.52	3.68	11767
	80% Grade stress	29.99	26.31	10.65	38.02	2.95	9414

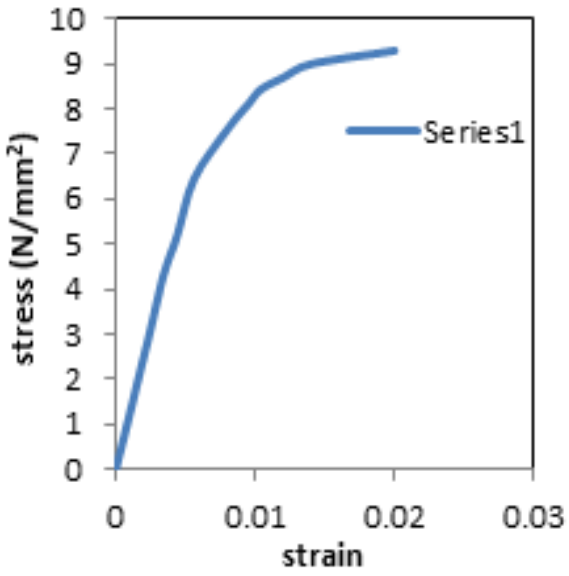

Figure 2 Typical Tensile Stress-Strain curves for Neem timber

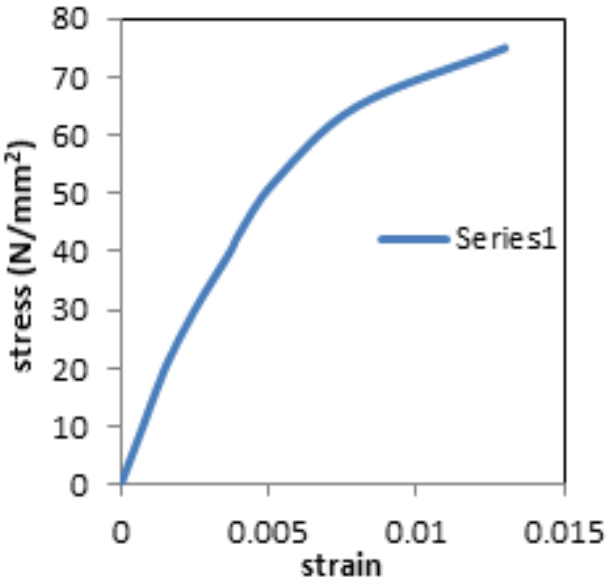

Figure 3 Typical Tensile Stress-Strain curve for Negro Pepper timber

Tables 5 Statistical significant result for Neem and Negro Pepper timber species

	Neem timber *(Azadirachta indica)*			Negro Pepper *(Xylopia aethiopica)*		
Mechanical property	Statistical F	Statistical P	Comment (significance difference at α=0.05)	Statistical F	Statistical P	Comment (significant difference at α=0.05)
Static bending	2.146	0.130	P>α not significant	1.095	0.393	P> α not significant
Compression parallel to grain test	3.146	0.050	P= α significant	1.063	0.403	P> α not significant
Compression perpendicular to grain test	3.685	0.034	P< α significant	0.722	0.524	P> α not significant
Tension parallel to grain test	8.829	0.001	P< α significant	2.634E0 3	0.000	P< α significant
Hardness test (Radial direction)	4.213	0.022	P< α significant	5.283	0.051	P> α not significant
Hardness test (Tangential direction)	0.078	0.925	P> α not significant	3.170	0.115	P> α not significant
Shear parallel to grain test	1.595	0.215	P> α not significant	1.183	0.369	P> α not significant

CONCLUSION

The timber species investigated, that is *Azadirachta indica* and *Xylopia aethiopica* possessed the physical and mechanical properties that are comparable to the properties of the existing timbers being used for construction purposes and therefore, the two timbers are suitable for structural engineering purposes. The various design values for the mechanical properties obtained will further promote the usage of the timbers in design and construction purposes.

REFERENCES

[1] Jozsef B. and Benjamin A.J., "Mechanics of wood and wood composites", Van Nostrand Reinhold Company New York, 1982,, pp 492

[2] Aguwa J.I and Sadiku S. . "Reliability Studies on The Nigerian Ekki Timber As Bridge Beam In Bending Under The Ultimate Limit State Of Loading ". Journal of Civil Engineering and Construction Technology Vol. 2(11), 2011, pp. 253-259, Available Online at Http://Www.Academicjournals.Org/Jcect

[3] Afolayan, J.O, Adeyeye, A.,. "Failure Analysis of a Glue-Jointed Roof Truss" , J. Eng. Appl. Sci., ISSN 1023-862, 17(1): 1998, 51-63

[4] Aguwa J. I., "Reliability Assessment of the Nigerian Apa (*Afzelia Bipindensis*) TimberBridge Beam Subjected to Bending and Deflection Under the Ultimate Limit State ofLoading" , International Journal of Engineering and Technology, (IJET) UK Volume 2, No. 6, 2012, pp1076-1088

[5] Kumar VS, Navaratnam V. "Neem (*Azadirachta indica*): Prehistory to contemporary medicinal uses to humankind". Asian Pacific Journal of Tropical Biomedicine 3(7), 2013.,505-514.

[6] Chattopadhyay RR, Chattopadhyay RN, Maitra SK. "Possible mechanism of anti-inflammatory activity of *Azadirachta indica* leaf extract". Indian J. Pharmacology. 25(2):, 1993,99- 100.

[7] Chattopadhyay RR. "Possible mechanism of anti-inflammatory activity of *Azadirachta indica* leaf extract": Part IV. Gen. Pharmacol. 27(3): , 1996 ,431-434.

[8] Chattopadhyay R.R, Bandyopadhyay M. "Effect of *Azadirachta indica* leaf extract on serum lipid profile changes in normal and streptozotocin induced diabetic rats. Afr. J. Biomed. Res. 8: , 2005, 101-104.

[9] Mamman P.H, Mshelia W.P, Susbatrus S.C and Sambo K.W. "Antibacterial effects of crude extract of *Azadirachta indica* against *Escherichia coli, Salmonella* spp and *Staphylococcus aureus"*.

International Journal of Medicine and Medical Sciences Vol. 5(1), 2013, pp. 14-18

[10] Hashmat I, Azad H, Ahmed A.. "Neem (*Azadirachta indica* A. Juss) - A nature's drugstore: An overview". International Research Journal of Biological Science 1(6), 2012 , 76- 79.

[11] Bempah K.C, Buah-Kwofie A, Asomaning J.. "Morphological studies of Neem *(Azadirachta indica* A. Juss.) seed and physicochemical properties of its oil extracts collected in Accra metropolis of Ghana". Elixir Applied Botany 39, 2011, 4951-4953.

[12] Sultana S, Khan MA, Ahmad M, Bano A, Zafar M, Shinwari Z.K. , "Authentication of herbal medicine neem (*Azadirachta Indica* A. JUSS.) by using taxonomic and pharmacognostic techniques. Pakistan Journal of Botany 43, 2011, 141-150.

[13] Jafari S, Saeidnia S, Ardekani MRS, Hadjiakhoondi A, Khanavi M. "Micromorphological and preliminary phytochemical studies of *Azadirachta indica* and *Melia azedarach"*. Turkish Journal of Botany 37, 2013, 690-697.

[14] Debashri M, and Tamal M. , "A review on efficacy of *Azadirachta indica* A. Juss based biopesticides: an indian perspective". Research Journal of Recent Sciences 1(3), 2012., 94-99.

[15] Uzodike E.B and Onuoha I.N. , "The Effect of *Xylopia Aethiopica* (Uda) on Intraocular Pressure". JNOA. Vol 16, 2010. Accessed on 10/12/2016.

[16] Aguoru C.U, Pilla C and Olasan J.O ,. "Phytochemical screening of *Xylopia aethiopica* with emphasis on its medicinally active principles. Journal of Medicinal Plants Research Vol. 10(22), 2016, pp. 306-309, available on http://www.academicjournals.org/JMPR

[17]Fleischer T., "*Xylopia aethiopica* A Rich: A chemical and biological perspective". J. Univ. Sci. Technol. 23: , 2003., 24-31

[18] Orwa C, A Mutua, Kindt R , Jamnadass R, S. "Anthony. Agroforest tree Database: a tree reference and selection guide version 4.0" , 2009, Available on (http://www.worldagroforestry.org/sites/treedbs/treedatabases.asp)

[19] John-Dewole O.O, Agunbiade S.O, Alao O.O, and Arojojoye O.A., "Phytochemical and antimicrobial studies of extract of the fruit of *Xylopia aethiopica* for medicinal importance", E3 Journal of Biotechnology and Pharmaceutical Research Vol. 3(6), 2012, pp. 118-122, Available online at http://www.e3journala s.org/JBPR

[20] Tona L, Kanbu K, Nigimbi N, Cimanga K, and Vietinck A.J. , "Antiamoebic and Phytochemical Screening of Some Congolese Medicinal Plants". Journal of Ethnopharmacol., 61(1):, 1999, 57 – 65.

[21] Esuoso K.O, Odetoun S.M., "Proximate Chemical Composition and Possible industrial Utilization of Blighia sapida seed and oils" , Journal of Phytotherapy Res., 72(7): , 2005, 311 – 313.

[22] Burkil H.M. "The Useful Plants of Wet Tropical Africa" , 4th Edition. Macmillan Press. 1, 1999, 34 – 36.

[23] BS 5268-2, "Structural use of timber Part 2: Code of practice for permissible stress design, materials and workmanship" , 2002.

[24] Ataguba C.O., Enwelu C, Aderibigbe W, Okiwe E.O. , "A Comparative Study of Some Mechanical Properties of *Gmelina Arborea*, *Parkia Biglobosa* and *Prosopis Africana* Timbers For Structural Use" International Journal of Technical Research and Applications E-Issn: 2320-8163, www.Ijtra.Com Volume 3, Issue 3 (May-June 2015), 2015., pp. 320-324 .

[26] Zziwa, A., Ziraba, Y.N. and Mwakali, J.A., , "Strength Characterisation of Timbers for Building Construction in Uganda", Second International Conference on Advances in Engineering and Technology, 2009, pp 450 – 456.

[27] British Standard, "Method of Testing Small clear specimens of Timber", The Timber Industry Standard Committee, 1957, pp 1-24

[28] Karlsen G. and Slitskouhov Yu, "Wooden and Plastic Structures", Mir publishers, Moscow, 1989.

[29] Ozelton E.C, Baird, J.A. "Timber Designer's Manual", British Standard Institution, 2 Park Street, London WIA 2BS, 1981, pp. 501.

[30] Desch, H.E., (1991), Timber properties, 6th Edition,Revised by J.M. Dinwoodie. Macmillan Education Ltd, London, pp 202.

[31] Findlay, W.P.K, "Timber properties and uses", Granada publishing company, London, 1978, pp 25.

[32] Engineering Achieves, "Brittle and Ductile Materials",2012,availableonhttp://www.engineeringarchives.com/les_mom_brittleductile.html , accessed on 30th April 2017.

[33] William N.(2004). Strength of Materials, Fourth Edition, Schaum's outline Series, Tata Micgraw-Hill Edition, New York pp 3.

CONCEPTUAL COST ESTIMATION OF ROAD PROJECTS IN ETHIOPIA USING NEURAL NETWORKS

Nardos Tadesse and Abebe Dinku
School of Civil and Environmental Engineering
Addis Ababa Institute of Technology, AAU

ABSTRACT

The rapid technological changes and advances in all business sectors strongly impose construction managers to facilitate their work through advanced software applications available to simplify different tasks. A research has shown that inaccurate cost estimation method is among the cause of cost overrun in the Ethiopian construction industry. This article presents conceptual cost estimation model developed using neural networks for federal road projects of Ethiopia. The conceptual cost estimation model developed has a mean absolute percentage error of 32.58% trained with only 48 exemplars. If the model is developed with the provision of enough data set to represent the road project with all-state of affairs, it is forecasted to improve the estimating capability of financers, employers and consultants. In addition, a friendly user interface is built to enable the utilization of the model developed easily and this article presents this interface with an example of actual road project in Ethiopia. The findings of this study indicate the prospect of application of neural network for cost estimation during early phase of the project development for Ethiopian road projects.

Key Words: Conceptual Cost Estimation, Neural Network, Parameters, Reliable estimate

INTRODUCTION

Reliable cost estimates are necessary for responsible cost management at every stage of a project. The application of advanced conceptual cost estimation tools in Ethiopian Construction industry is at an infant stage and requires localized researches. Cost overrun of infrastructure projects has become a common problem for the construction industry as recognized by industry researchers and practitioners [1].

The higher amount of budget allocated to the road construction industry stresses the requirement of applying advanced planning tools for project completion within estimated cost.

The Government of Ethiopia formulated the Road Sector Development Program (RSDP I to IV) in 1997 and disbursed 48.11 Billion Birr in the years 2011 and 2012 for the RSDP IV [2]. A research conducted by ERA Research Center on causes of cost overrun on Ethiopian Federal Road projects in 2016 showed that 10 to 21% of cost overrun is recorded [3]. This shows the requirement of measurement to be taken to improve cost estimate reliability.

A research revealed that inaccurate cost estimation method and poor planning are among the factors contributing to cost overrun in the Ethiopian construction industry [4].

In addition, the review of best practice, which is the research conducted by U.S. department of transportation Federal highway administration, showed that cost estimation programs and quality control & assurance programs are developed in light of addressing cost overrun issues [1].

This paper aims to use a similar approach and develop a conceptual cost estimation model for Ethiopian road projects through the application of Neural Network. Therefore, identification of factors that affect total cost, which are to be used as parameters in training a Neural Network model, is the first objective.

The chief goal is to support decision makers through increased reliability of estimated cost of road construction projects at early stages of project development by providing cost estimation tool.

LITERATURE REVIEW

Conceptual Cost Estimation

A conceptual estimate is made during early phase of project development without detailed design and engineering data, and with limited information on project scope. Therefore, considerable experience and judgment are required to obtain a dependable approximate estimate for the cost.

Estimating is the heart of the cost engineer's work and consequently, it has received appropriate attention over the years. The first function of a conceptual estimate is to tell the owner about the anticipated cost, thus presenting useful information for the owner in contemplating the project feasibility and further development [6]. Conceptual and preliminary estimates are made for several reasons, including [7] [8]:

- Feasibility studies
- To establish a basis for financing, appropriation of funds or validation of project budgets
- Appropriation of the project scope and selection from alternate design and investment
- Presentation of bids and tenders which is to establish a benchmark for a construction bid

Cost Estimating Methods

Cost Estimating methodologies fall into one of the following four categories discussed below [5].

Historical bid-based Estimation

Historical bid-based methods are commonly used to develop engineer's estimates, and are applied when the project design progressed enough to provide quantities of unit of works. Historical unit costs are applied to estimate the total cost of each work items [5]. **Cost based Estimation**

Cost-based estimate methods are based on calculation of unit costs for each project with details of labor, equipment, material and specialty contractor estimation for each item of work. Historical bid data are not utilized [5]. Cost-based estimates require significant effort, time, and estimator experience to prepare.

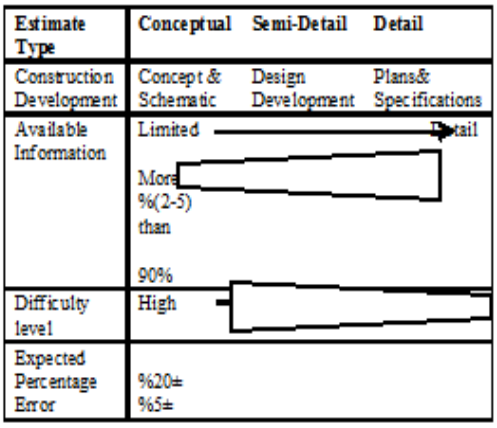

Fig.1: Construction cost estimating methods [9]

They should be limited to those items that comprise the largest cost percentage of the project, typically that 20% of items of work that account for 80% of project cost. The cost of the remainder of estimate line items can be determined using Historical Bid-Based Estimate methods [11].

Risk-based

Risk-based estimate methods include complex probabilistic analysis with identification of opportunities and threats related to cost, schedule, and events related to the project. It uses different techniques, such as historical data, cost based estimating, and the best judgment of subject matter experts for given types of work [5].

Information Available during Conceptual Project Development Level

The information available is one of the distinctive features of the different types of cost estimates. The estimate level among the different types of estimates available does not give clear and definite boundary. Due to this reason, there are some literatures that use the terms conceptual and preliminary estimate interchangeably. During the conceptual phase, general information about the project will be available such as the road length, road width from standards, the location of the project and the project scope.

And a parametric cost estimation technique can be deployed from historical costs of similar past projects. During the preliminary phase, preliminary quantities of earthwork and pavements are available by the use of digital terrain model and different maps. Figure 1 below shows the available information, difficulty level and expected percentage error for different types of cost estimates.

The identification of the influential factors or parameters affecting total project construction cost is necessary to develop cost estimating model. The input parameters identified through literature review of road construction cost estimation are summarized below in table 1.

Artificial Neural Network

Artificial intelligence is defined as: "The study of how to make computers do things at which, at the moment, people are better" Rich and Knight, 1991

Artificial Intelligence is the branch of computer science that is concerned with the automation of intelligent behavior and seeks to explain and emulate intelligent behavior in terms of computational processes [15]. Artificial Neural Networks (ANNs) are a functional abstraction of the biologic neural structures of the central nervous system [16].ANN generally learns from "experience", rather than being explicitly "programmed" with rules like in conventional artificial intelligence [17].

Benefits and limitations of Artificial Neural Network

The use of neural networks offers the following useful properties and capabilities [18]:

Input-output mapping: a popular paradigm of learning called supervised learning involves the modification of the synaptic weights (free parameters) of a neural network by applying a set of training samples. Thus the network learns from the samples by constructing an input-output mapping for the problem at hand.

i. Adaptive: Neural networks have a built-in capability to adapt their synaptic weights to changes in the surrounding environment.

ii. Contextual information: contextual information is dealt with naturally by a neural network.

Fault tolerance: a neural network has the potential to be inherently fault tolerant.

- To predict acceptability of a new technology, cash flow, construction demand, construction budget performance and construction cost
- To investigated the overhead cost practices of construction companies in Saudi Arabia
- To develop cost estimating model for the structural systems of reinforced concrete buildings in the sense that its performance is degraded gracefully under adverse operating. Although the artificial neural networks have many advantages, on the other hand their accuracy highly depends on the quality of the trained data and the ability of the developer to choose truly representative sample inputs. In addition, trial and error method used to obtain the formula to decide what architecture of ANN should be used to solve the given problem and which training algorithm to use.

Application of ANNs in Construction Engineering

The most common application of ANNs in the construction management area is prediction. Few of the applications of the ANN in construction management for prediction and estimation in construction engineering are given below [9, 16]:

- Model for predicting increase in time and cost of construction projects in Egypt
- To forecast actual cost of a project based on the earned value management system
- To estimate conceptual cost of Libyan Highway Projects

The literatures show the vast application of ANN in the construction industry worldwide and the need of the Ethiopian construction industry to advance in order to cope up with the rapid and dynamic advancement of technology is undeniable.

Table 1: Previously used parameters by other research papers [9, 12, 13, 14]

Year	Research description	Input parameters
1998	Neural network approach was used to determine highway construction cost in Canada	Project type, project scope, year, construction season, location, duration, size, capacity, water body, and soil condition.
2005	Multiple regression model and ANN model were used to estimate the cost at conceptual phase of highway projects in Poland and Thailand.	Predominant Work Activity (Asphalt or Concrete), Work Duration, Pavement Width, Shoulder Width, Ground Rise Fall, Average Site Clear/Grub, Earthwork Volume, Surface Class (Asphalt or Concrete), and Base Material (Crushed Stone or Cement Stab).
2013	Parametric Cost Estimation of Road Projects Using Artificial Neural Networks in Palestine	Project scope, Water networks, Pavement type (asphalt or interlock), Pavement area, Length of the road, Length of the curbstones Lighting networks, Sewage networks
2013	Conceptual Cost Estimate of Road Construction Projects in Saudi Arabia by developing regression models to predict the total construction cost of a road project in the early phases.	Earthwork; cut and fill (m3), Base works (m2), Asphalt works (m2), Road length, Road width (m)
2014	Testing regression models to estimate costs of road construction projects, to develop early cost estimating models of road construction projects in Ethiopia	Earthwork; cut, fill, and topping quantities (m3), Sub base and Base coarse quantity (m3), Asphalt quantity (m2), Road width (m), Road length (m)

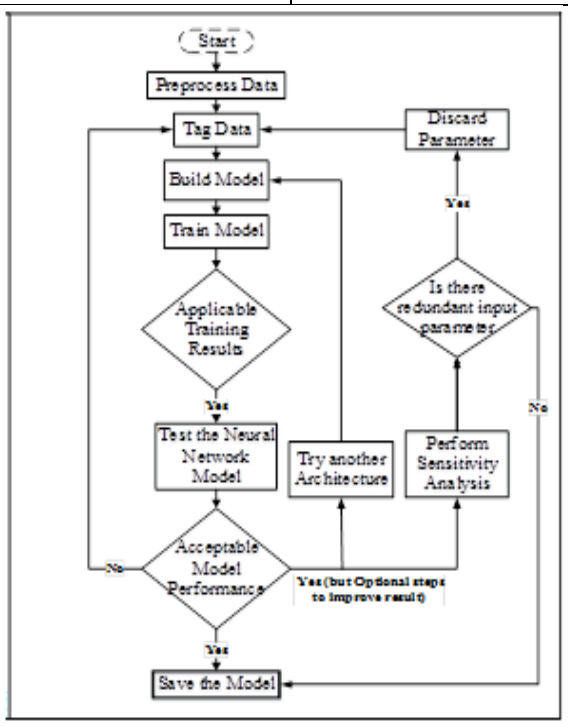

Fig 2: Model development procedure

RESEARCH METHODOLOGY

The research methods applied for this research are correlational descriptive and quantitative research methods. Correlational studies trace relationships among two or more variables in order to gain greater situational insight. Therefore to identify the parameters to be used for developing the cost estimation model correlational descriptive research method was adopted. The quantitative research method was adopted to develop the model that estimates cost.

The study area of this research is Ethiopia excluding the capital city, Addis Ababa. Addis Ababa is the most urbanized, highly congested and populated area fading the resemblance and similarity of the road construction cost among the other areas. Most of the road networks are built up which has a significant influence of right of way issues affecting construction periods and work progress which in turn influences the project cost. The road projects taken as historical feed to develop the parametric cost estimation are from the North, South, East, West and Central region. The central region includes road projects in 250KM radius from Addis Ababa city. The principal tools applied are Microsoft Excel 2013, Neuro Solutions version 7.1.0.0, and Visual Basic Application.

Research procedures

The study started with an intensive literature review and consequently data were collected. The data collection was conducted in two phases as preliminary data collection and final data collection. The preliminary data was collected through 13 experts' interview in open and close ended questions. The experts interviewed include Highway Engineers, Contract Administrators, Quantity Surveyors, University Lecturers and from client side, Project Team Leaders

and Counterparts from ERA. The analysis of the preliminary data collected was carried out for the sole purpose of identifying and determining input parameters. This stage was imperative as not to escape any important parameter that may affect cost of road projects. The next step was the collection of final data to be used as historical basis for parametric estimation. The collected data were compiled from Ethiopian Road Authority Management System (ERAMS), contract documents and reports. A total of 58 data were collected for the model development. The data were then analyzed and put in table format for simplicity and avoidance of double use of specific project.

The succeeding step was development of the neural network model by training the program. Then the model was tested and sensitivity analysis was carried out. A friendly interface was then created to link the neural network model with users. Finally, conclusions were made and recommendations were forwarded in subgroup of the party aimed to be addressed.

MODEL DEVELOPMENT

The cost estimating models are developed in series of steps as shown in Figure 2.

The preprocess of data in this paper is designated to arranging the data in rows and columns, encoding the data, randomizing the data and conveying the total project costs to a common base year. NeuroSolutions creates a new breadboard with typical elements used for neural network configurations chosen and the breadboard is saved. The breadboard created is shown in Figure 3. The chosen models for this research include linear regression, multilayer perceptron and generalized feed forward. NNs are then trained using available data to understand the underlying pattern. During training, both the inputs, representing problem parameters and outputs, representing the solutions are presented to the network normally for thousands of cycles. At the end of each cycle, or iteration, the network evaluates the error between the desired output and actual output.

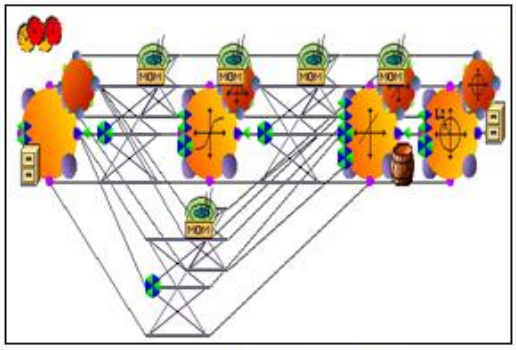

Fig. 3: Snapshot of breadboard created for the conceptual cost estimation model

Then this error is used to modify the connection weights according to the training algorithms used [9]. Back propagation is the type of algorithm adapted, which is a common method of teaching artificial neural networks and uses supervised learning.
The trained network is tested with the data set designated for testing and the network with the best performance is chosen. The performance measures include Mean Square Error (MSE) and Correlation Coefficient (r). Finally a sensitivity analysis was carried out.

ANALYSIS AND DISCUSSION

The analysis and discussion is comprised of three subsections over which preliminary data collected, final data collected and the results of the model developed are analyzed and discussed in detail.

Analysis and Discussion on Preliminary Data Collection

The preliminary data collected was analyzed with the aim of identifying the influential parameters affecting road project cost during conceptual stage. One of the findings of the interview is that two estimate models can be predicted during the early phase of the project, which are conceptual and preliminary estimates. This article only focuses on the conceptual estimation level. The detailed analysis, discussion and results of the preliminary cost estimation model are given on the research paper submitted to Addis Ababa Institute of Technology [19]. The parameters affecting conceptual cost of Ethiopian road projects are briefly discussed.

The parameters identified for the conceptual estimation model are Project location, Project scope or type, Wearing Surface Class, Road length and width, Terrain classification, Project delivery system and Structure intensiveness.

Terrain classification and Structural intensiveness are discarded and taken as a limitation and are recommended for future studies because they could not be compiled for all project data collected. This is because the ERAMS (Ethiopian Road Authority management System) software did not include this parameter as an output report of the system even though the data was initially feed to develop the software.

The two project delivery systems predominantly used in the Ethiopian road construction are design-bid-build (DBB) and design-build (DB). The estimation structures of the two are totally different and therefore project delivery system was not used as a parameter. Therefore, the scope of this study is DBB projects for the reason that only DBB project's data were collected.

Project location required further study on how to classify the location of the study area. The study area of this paper is Ethiopia excluding Addis Ababa. The concerns taken into consideration for classification purpose in this study are climate and sources of four construction materials, which affect construction cost and time. The study was started with an assumption and then the assumption was proven. The assumption was for the location classification to be the same as ERA's regional administrative organization as North, South, East, West and Central region.

The first point of consideration taken to prove the assumption is climate. Rainfall is the major climate measure, as discussed in ERA manual 2013. The rainfall distribution of Ethiopia supports the justification of the assumption as shown with the broken lines on the map below of Figure 4.

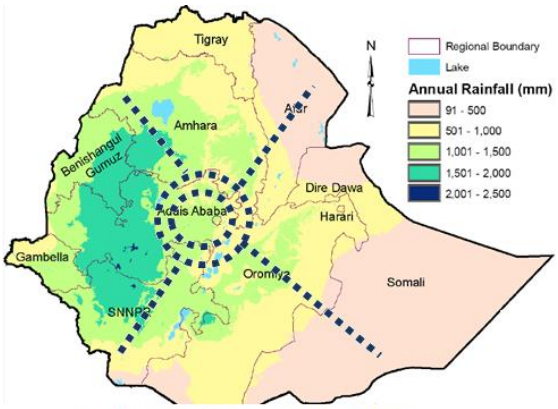

Fig.4: Rainfall distribution of Ethiopia with location categorization [20]

The second accounted point on proving the assumption is the sources of construction materials. The travel distance and cost for

transportation of materials depends on the distance between the material manufacturing (importing site) and the construction sites. For instance a road project located in Dire Dawa will have less bitumen transportation cost than a project located in Gambella. This can be easily seen on Figure 5.The materials taken into consideration are asphalt bitumen, cement, fuel and steel reinforcement bars.

Cement is one of the materials used for concrete production mostly for structures in road construction. According to a report of the presentation on the 7th Africa Cement Trade Summit in 2015, the Ethiopian cement industry experiences insignificant import that is only limited to special cements [21]. Therefore the supply of cement for the road construction is from local manufacturers. Dangote, Derba, National, Messebo, and Mugher cement factories are the major suppliers. Figure 5 shows the distribution of the factories is not uniform thought out the country which results in different cement transportation cost along the regions. This similarly supports the assumption of location categorization as north, south, east, west and central region.

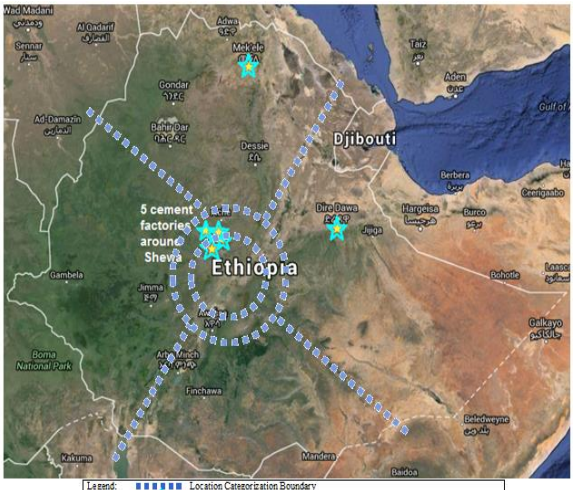

Fig.5: Distribution of Cement factories in Ethiopia in location categorization [22]

From the above discussions, location is determined to be used as influential parameters for conceptual road project cost estimation in the subdivision of south, north, east, west, and central regions. The project scopes that are taken into account by this study are new construction of roads and upgrading of existing roads. Construction duration refers to period of road construction staring from commencement to completion. Construction year in this research refers to the year of construction commencement which is identified as a parameter on this study based on previously executed researches. The year of construction is related to price escalation taking into account the supply and demand balance of the market and inflation rate. The year of construction was used to convey the total project costs to a common base year of 2006 through the application of consumer price index (CPI) from Central Statistical Agency of Federal Democratic Republic of Ethiopia, based on available data as presented on Table 2. The road length and width were identified as an input parameter during literature review and fully supported by the interview. The road length was used to develop the estimation model. But the width was castoff due to the reason that data collected on road width shows that more than 90% of the data is similar. Therefore it was discarded and not used for the model development.

Table 2: Consumer Price index for construction projects.

Year	Consumer Price Index
2006	100.0
2007	112.0
2008	136.6
2009	160.0
2010	195.7
2011	219.4
2012	245.1
2013	267.9
2014	292.3

Analysis and Discussion on Final Data Collected

The final data collection resulted in production of set of data to be used as historical feed for analogous parametric estimation. Totally 58 data were collected and out of these 48 data

were used for conceptual estimation model development. The rejected data were not able to be used for model development due to incompleteness of data, inconsistency of data, and because of being on-going project data. The percentage distributions of the data set in terms of location are shown in Figure 6.

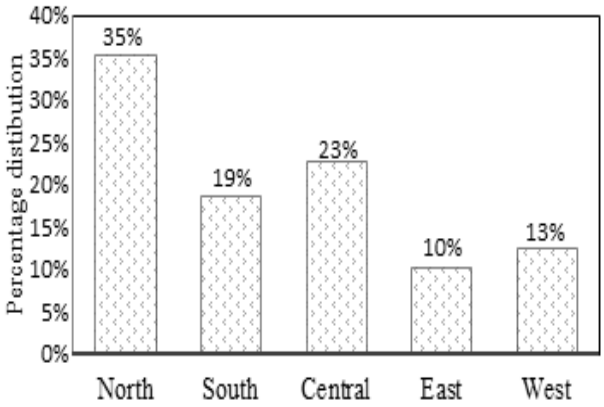

Fig.6: Percentage distribution of location subgroup for conceptual estimation model

Depending on the percentage distribution of data set for location, the north area outshines accounting for the 35% and on the other hand the data set from east region accounts for 10% of the total data set.

Figure 7 shows the percentage of data collected with respect to surface class, which are classified as Asphalt Concrete, Double Bituminous Surface Treatment and Gravel Wearing Course

Discussion on Model development

The percentage of row tags have been varied while training the network to get best accuracy of the models with respect to the performance measures given in testing reports. The data tags of the two models are shown in Tables 3 below.

Training Result discussion

After building a neural network breadboard the next task performed was training the network to develop a model. The training result presented below in Figure 9 shows the best network weight which is saved at the

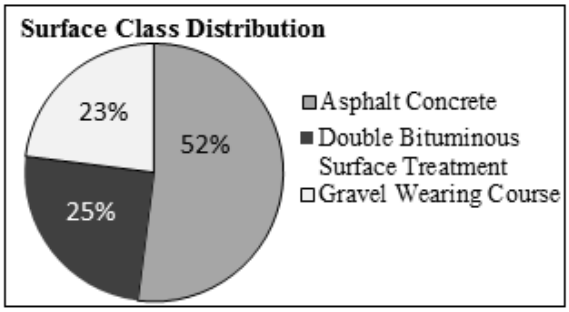

Fig.7: Surface class distribution of data set

The study took the actual completion date and commencement date of the projects to compute the duration, therefore the actual period of construction is taken. The project road length is the other parameter encompassed in the model. The length distribution of the project data collected is shown in Figure 8 after being classified into four.

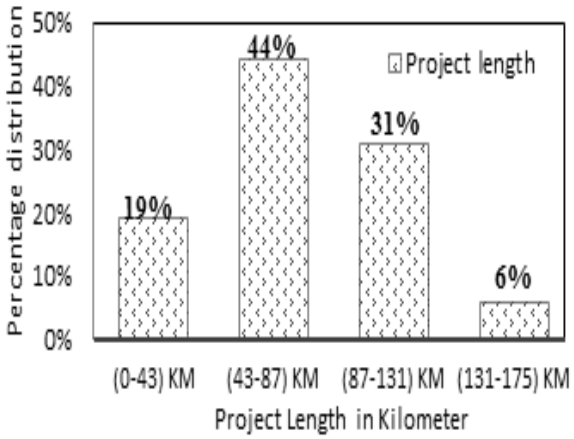

Fig. 8: Percentage distribution of data with length

epoch when the cross validation error is minimum for conceptual cost estimation

Table 3: Input/output tags and Percentage of raw tags

Input tags	**Output tag**	**Row tags**	**% of row tags**
Project Location Project Scope Wearing Surface Class Road Length Duration	Total Road Construction Cost	Training Cross Validation Testing	70% 10% 20%

model developed. As it is shown in the figure, the training of network stopped after training and cross validation means square errors (MSE) have reached the minimum and kept constant for continuing trials. The training result of the model shows the MSE approached minimum during the early phase of trials or epoch. After many trials were performed, the neural network configuration or topology with the best performance measure for the conceptual estimation model is Regression General Feed forward network with the architecture of GFFR-1-O-M. The architecture represents a Regression General Network with one hidden layer, Momentum Gradient search and On-line learning updates method. The networks trained were then tested with the provided testing data sets to the performance of the models.

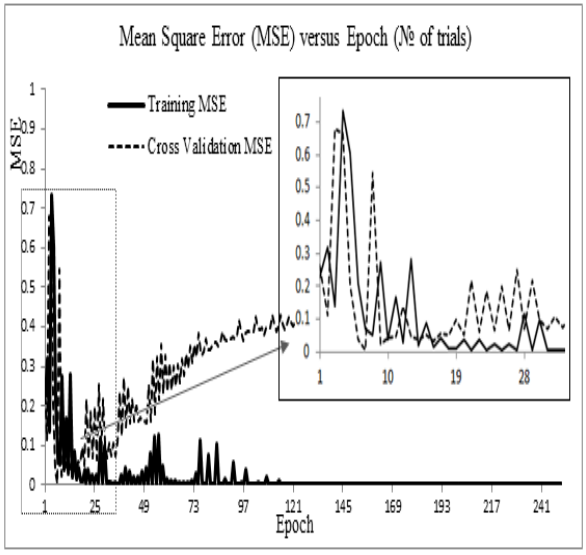

Fig.9: Training report showing MSE values for Conceptual estimation model

Test Results discussion

The model was trained with 48 exemplars and 33 of the exemplars were used for training; 5 of the exemplars were used for cross validation to produce better output for unseen examples; and 10 of the exemplars were used for testing. Figure 10 below shows the desired output and network output of the conceptual cost estimation model developed converge in the same direction in close proximity.

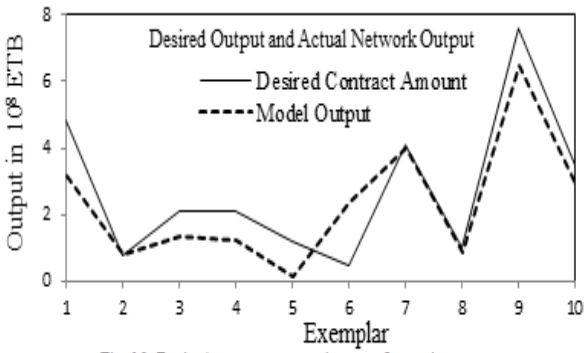

Fig. 10: Desired output to network output for testing exemplars of Conceptual and model

Coefficient of determination denoted as r^2 of network output verses desired graph, which is equal to 0.82, shows that the network put fits the desired output and moves in the same direction, as given on Figure 11. With the provided number of data set, these are promising results towards the possibility of better accuracy with provision of more data points.

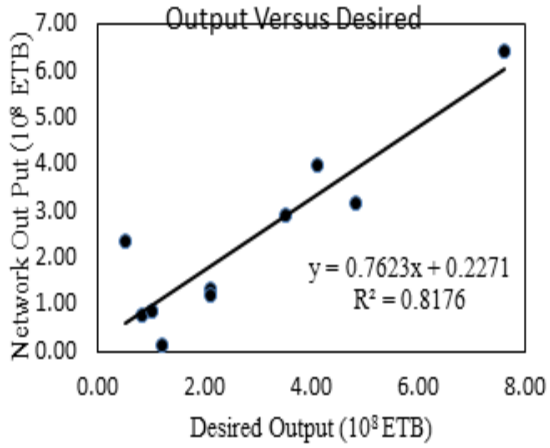

Fig. 11: Scatter plot of desired output Verses network output for testing exemplars

Sensitivity Analysis Result

The sensitivity analysis was carried out for the estimation models that was trained and tested. To carry out the sensitivity analysis the inputs are varied between its mean ±1 of standard deviations while all other inputs are fixed at their respective means. This is done for 50 steps to each side. A report is then generated which summarizes the variation of each output with respect to the variation in each input parameter. The report is presented in Figure 12 below.

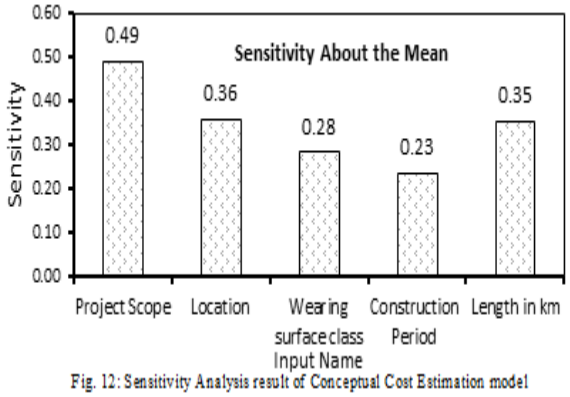

Fig. 12: Sensitivity Analysis result of Conceptual Cost Estimation model

As it is seen on the chart above construction period has the lowest effect on the model; however this parameter was not eliminated or discarded due to the reason that the model was developed for projects completed over different period of years. Project scope and road length have the highest effect of the model. With the number of exemplars provided under consideration, the sensitivity analysis result shows that all the parameters used have indisputable impact on the total construction cost.

Discussion on the Expected Accuracy of the model

The main performance measures this study used to evaluate the performance of the model and to reflect the application of ANN for conceptual cost estimation in Ethiopian road projects are percentage expected and mean absolute percentage errors.

The mean absolute percentage error of the conceptual cost estimation model calculated for the 48 exemplars is 32.58%. This is a very encouraging result with the provided set of exemplars. The model is performed with only 48 exemplars which is not nearly enough to represent road projects in Ethiopia. It is, therefore, predicted to improve with the provision of sufficient data to support all state-of-affairs of each input parameter identified to affect total project cost as a representative sample. The ANN model developed on this research cannot be readily used in the industry but this research is an indication to the prospect of application of ANN for cost estimation of Ethiopian road projects during early phase of the project development.

Structuring User Interface

The friendly user interface is created to use of the model by simply entering the input parameters and receive the predicted total cost is shown in Fig. 13.

Fig. 13: Snapshot of User Interface built

with an example of an upgrading road project cost estimate. The actual contract amount for the construction of the road project is 1,142,567,660.95 ETB. Therefore, the mean absolute percentage error calculated using the actual and desired value is 9% for this numerical example.

CONCLUSIONS

The research was conducted to provide the road construction industry with a computerized and high-tech tool that can estimate cost during the early phase of project development. The conclusions drawn from this research are summarized as follows:

1. Neural Networks have been used in construction engineering and management for prediction and decision-making globally. However advanced technological tools applied worldwide that can expand construction management roles are not fully exhausted and exploited by the Ethiopian road construction industry.
2. Based on the data analysis and discussion the influential parameters for conceptual stage include

construction duration, location, wearing surface class, project scope, terrain classification, structural intensiveness, road length and year of construction.

3. The mean absolute percentage error of the conceptual cost estimation model developed is 32.58%, which has proven that Neural Network is a promising tool for use in the initial stages of Ethiopian road construction projects, providing construction managers access to well-organized and scientifically systemized historical cost data of similar projects on local basis.
4. The application of this cost estimation tool increases accuracy of the cost estimates.

Significantly through the minimization of assumptions cost estimators have to draw due to the existence of low information availability during the initial phase.

RECOMMENDATIONS

The aggregate recommendations drawn are summarized below in a category of the party that is aimed to be addressed.

Decision-Makers in Ethiopian Road Construction Industry

Decision makers of the industry include road authorities, financers and policy makers on road construction in Ethiopia. The applications of advanced project cost estimation tools currently in use by the developed world are relatively at an infant stage in Ethiopian road construction relatively. Therefore it is recommended that authorities embrace and adapt such computerized cost estimation techniques to be applied during early phase of project development. Therefore, the provision of supporting policies along with implementation and enforcement technique establishments that will enable the use of reliable cost estimation tool is recommended.

Baseline for Future Research

The discarded input parameters in this research due to unavailability of data which are project delivery system, structural intensiveness and terrain classification should be further studied.

As mentioned above advanced cost estimation tool can also be applied to Ethiopian building construction projects. For instance the Ethiopian government is currently working towards provision of condominium apartments to the vast urban population. Therefore, future researches can be made in developing cost estimation models for construction of building project.

REFERENCES

[1] Sirous A. and Michael P., "*Highway project cost estimating and management, The U.S. department of transportation Federal highway administration,"* The State of Montana Department of Transportation in cooperation with The U.S. Department of Transportation Federal Highway Administration, February 2009

[2] Ethiopian Roads Authority, Report on "*Assessment of 15 years performance of Road Sector Development Program*," ERA, Ministry of Transport, The Federal Democratic Republic of Ethiopia, January 2013

[3] Yinges T., "*Causes of Cost and Time Overrun on ERA Road Construction Projects*," ERA Road Research Center, Ethiopia, 2016

[4] Zinabu T., "*Causes of Contractor Cost Overrun in Construction Projects: The Case of Ethiopian Construction Sector,"* International Journal of Business and Economics Research, Vol. 4 Issue 4: p180-91, August 2015

[5] Ministry of Transportation and Infrastructure Project Management Support Services: "*Project Cost Estimating Guidelines*," Version 01.02: p20 September 30, 2013

[6] Jelen, F. and Black J., "*Cost and Optimization Engineering,"* 2nd edition, McGraw-Hill, New York, 1983

[7] Ibrahim M., "*Conceptual Cost Estimate of Road Construction Projects in Saudi Arabia*," Jordan Journal of Civil Engineering, Vol. 7, Hail University, KSA, 2013

[8] Michael D., Dell I., "*The Architect's Handbook of Professional Practice: Detailed Cost Estimating*," 2003

[9] Hasan J., M.Sc. Thesis on "*Parametric Cost Estimation of Road Projects Using Artificial Neural Networks,"* Gaza Deanery of Graduate Studies, Faculty of Engineering, Civil Engineering Department, Construction Management, The Islamic University, Gaza, 2013

[10] Emad E., Lecture note on "*Construction Project Management," Structural Engineering*

Department, Faculty of Engineering, Mansoura University," November 2015

[11] Strategic Assessment and Estimating Office (SAEO) in alignment with the goals of the Statewide Program Management Group (SPMG): *"Cost Estimating Manual,"* p11, Washington State, November 2008

[12] Shihunegn A., M.Sc. Thesis on "*Testing Regression Models to Estimate Costs of Road Construction Projects in Ethiopia"* School of Graduate Studies, Construction Technology and Management, Addis Ababa Institute of Technology, 2014

[13] Amr A., *"Parametric Cost Estimating of Highway Projects using Neural Networks,"* Faculty of Engineering & Applied Sciences, St. John's Newfoundland, Canada, July 1997

[14] Ibrahim M., *"Early Cost Estimating for Road Construction Projects Using Multiple Regression Techniques,"* Australasian Journal of Construction Economics and Building; Vol. 11 Issue 4, 2011

[15] Stuart J. Russell and Peter N., *"Artificial Intelligence: A Modern Approach, Prentice Hall, Englewood Cliffs,"* New Jersey, 1995

[16] Megha J. and Pathak K., *"Applications of Artificial Neural Network in Construction Engineering and Management,"* International Journal of Engineering Technology, Management and Applied Sciences, Volume 2 Issue 3, August 2014

[17] Megha J. and Pathak K., *"Applications of Artificial Neural Network in Construction Engineering and Management,"* International Journal of Engineering Technology, Management and Applied Sciences, Volume 2 Issue 3, August 2014

[18] Carsten P. and Thorsteinn R., *"An Introduction to Artificial Neural Networks,"* University of Lund, Sweden, 1991

[19] M. Hajek, "*Neural Networks,"* Neural networks.doc, University of KwasZulu-Natal, 2005

[20] Nardos T., M.Sc. Thesis on "Application of Artificial Neural Network for model development of Conceptual Cost Estimation of Road Projects in Ethiopia," Construction Technology and Management, Addis Ababa Institute of Technology, Addis Ababa University, July 2016

[21] Ethiopian Road Authority Manual, "*Site Investigation, Physiography, climate, geology and soil distributions categorization Manual,"* 2013

[22] Gemechu W., Presentation on "*Challenges and prospects of Ethiopia's cement industry: Strategic perspective*," Construction review online By Africa for Africa, April 28, 2015

[23] Google Earth, Search: "Dangote, Derba, National, Messebo, and Mugher cement factory in Ethiopia," Accessed on April-May, 2016, https:/ /www.google.com/earth

Parametric Investigation and Survey of Spintronic Sensors v-s Electronic Sensors (Case study: Current sensors)

Ephrem Teklu[#1], Getachew Alemu[#2]
[#1] *Addis Ababa University, Addis Ababa Institute of Technology, School of Electrical and computer Engineering, Addis Ababa, Ethiopia*
ephrem2009@yahoo.com

ABSTRACT

Conventional electronic devices depend on the transport of electrical charge carriers–electrons in a semiconductor such as silicon [1]. Now, however, physicists are trying to exploit the 'spin 'of the electron rather than its charge to create a remarkable new generation of spintronic devices which are smaller, more versatile and more robust than those currently making up silicon chips and circuit elements. Compared with other solid-state sensors, spintronic sensors offer more sensitivity and precision and are not damaged by large magnetic fields. This paper presents the investigation results of the comparison of the conventional electronics current sensors and spintronics current sensors relying on the sensitivity of the two. To extract our conclusion survey of the researches on spintronics sensors and conventional electronic sensors are done separately.
Keyword: Conventional electronics, spin, GMR, current sensor, Magnetic Bipolar Transistor

INTRODUCTION

Existing semiconductor electronic and photonic devices utilize the charges on electrons and holes in order to perform their specific functions such as signal processing or light emission.

Spintronics, also called magneto-electronics or spin-electronics is a branch of physics engaged with the storage and transfer of information by active manipulation of electron spins in addition to electron charge, to process electronic data in solid-state systems [4].

Like any other conventional electronics equipment, electronic sensors as well, are relatively large in size and consequently their cost is large. In addition, their operation need substantial amount of power. To overcome this, industry continues to reap the benefits of solid state magnetic field sensing. Every day new applications are found for solid state magnetic field sensors due to their small size, low power and relatively low cost. This brings the spintronics technology in to application.

THEORETICAL BACK GROUND

Spin and Spintronics

An electron has two attributes, "charge" and "spin". Spin is an intrinsic quantity of the angular momentum of electrons, treated as if they were tiny spinning balls [5], as shown in Fig.1.below.

In today's world of computers which is based on conventional electronics, we have either an ON or OFF, (1 or 0) or (UP or DOWN) state, the in-between states being ignored. But in spintronics with the spin of electron we can have many states and the two states limitation can be overcome. For this reason, in spintronics, large amount of information can be processed a whole lot faster. The relative number of electrons with spin-up and spin-down is very important for the magnetic properties of a chosen material. Nonmagnetic materials are characterized by the same number of electrons having the same properties in both (up/down) spin channels, while in magnetic materials there is an imbalance in the density of states for spin-up and spin-down electrons [6].

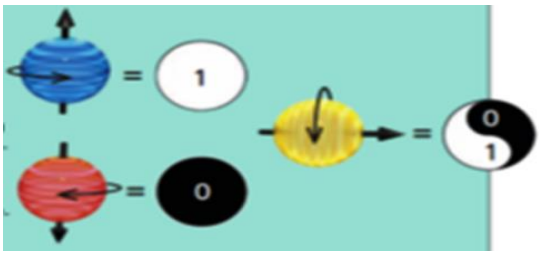

Fig. 1. Quantum representation of Spin [5]

Among recent advances in spintronics, magnetic tunnel junctions have been under intensive study

and are poised to become one of the most widely used spintronic devices.[7].

Successful application of the wide range of possible spin dependent phenomena in semiconductor systems requires: effective and efficient techniques for electrical injection of strongly spin-polarized currents, transfer of electrons without losing their spin, as well as electrical detection of such spin current.

2.2. Basic Electronics and Spintronics Devices Modeling

i). Conventional P-N Junctions: Conventional spin-unpolarized p-n junctions are semiconductor material whose left side is p-type, doped with N_a acceptors per unit volume, and whose right side is n-type, doped with N_d donors per unit volume. At V = 0, the generation current j_{gn} due to thermal excitation of an electron-hole pair, and the recombination current j_{rn}, due to the thermal activation of the electrons are in equilibrium, i.e., $j_{gn} = j_{rn}$ and there is no net currents flow [8]

$$j_{gn} = -j_{rn}\,(V = 0) = -KN_d\left(e^{-qV_b/K_BT}\right) \quad (1)$$

$$j_n = j_{gn} + j_{rn} = j_{gn}\left(e^{qV_b/K_BT} - 1\right) \quad (2)$$

$$j_p = j_{gp} + j_{rp} = j_{gp}\left(e^{qV_b/K_BT} - 1\right) \quad (3)$$

Where: K is constant, N_d-density of electrons, q - magnitude of the electron charge, V_b- threshold voltage, T-temperature, k_B – Boltzmann's constant. j_{gn} and j_{rn} are the generation and recombination currents due to electrons respectively, and j_{gp} and j_{rp} are the generation and recombination currents due to holes respectively. j_n and j_p are the electron and hole current densities respectively.

Putting electrons and holes together, we finally obtain the I-V characteristic equation of a p-n junction in the form,

$$j = j_g\left(e^{qV_b/K_BT} - 1\right) \quad (4)$$

where j is the current density in the p-n junction and

$$j_g = j_{gn} + j_{gp}$$

ii). Magnetic diode: At the junction of magnetic and non- magnetic semiconductors there is a source of non-equilibrium spin in the junction. The source can be either electrical or optical. For simplicity we consider only one type of magnetic diodes, those with magnetic p-region. We further assume that holes are spin unpolarized, since holes, due to their strong spin-orbit coupling, usually lose their non-equilibrium spins very fast in comparison to electrons.

The generation current is different for spin-up and for spin-down electrons. The same is true for the recombination current. This current can be controlled by magnetic field, modifying the splitting of the electron bands in the magnetic region, or by introducing non-equilibrium spins in the n-region. [8].

The electron recombination current, jrn, in the magnetic diode is jrn↑+jrn↓ where jrn↑ is the recombination current of the spin-up electrons and jrn↓ is the recombination current of the spin-down electrons.

Suppose the equilibrium spin polarization of electrons in the p-region is P_0, and the non-equilibrium spin polarization in the n-region, due to a spin source, is δP. Then the spin-up and spin-down electron currents are [8],

$$j_{rn}\uparrow = 1/2\ K\,(1 + P_0)\ (1 + \delta P)\,N_d\left(e^{q(-V_b+V)/K_BT}\right) \quad (5)$$

$$j_{rn}\downarrow = 1/2\ K\,(1 + P_0)\ (1 + \delta P)\,N_d\left(e^{q(-V_b+V)/K_BT}\right) \quad (6)$$

where all the parameters are as defined in the previous discussion.

The generation current does not depend on non-equilibrium conditions. This means that,

$$j_{gn}\uparrow = -j_{rn}\uparrow\ \ (V = 0, \delta P = 0) = -\ 1/2\,K\,(1 + P_0)\,N_d\left(e^{qV_b/K_BT}\right) \quad (7)$$

$$j_{gn}\downarrow = -j_{rn}\downarrow\ (V = 0, \delta P = 0) = -\ 1/2\,K\,(1 + P_0)\,N_d\left(e^{qV_b/K_BT}\right) \quad (8)$$

Summing up all the contributions to the electron current we obtain [8],

$$j_e = j_{gn}\left[e^{qV_b/K_BT}(1 + P_0\delta P) - 1\right] \quad (9)$$

The above equation expresses spin-charge coupling in magnetic p-n junctions [8]. For a parallel orientation of the spins, the current is enhanced; and for an antiparallel orientation, the current is reduced. The relative change of the current with respect to the orientation of the equilibrium and non-equilibrium spin gives rise to a giant magneto resistive (GMR) effect in magnetic diodes. The current is either positive or negative, depending on the sign of the product of $P_0\delta P$. This phenomenon is called spin-voltaic effect producing an emf from non-equilibrium spin [8]. The spin-voltaic effect is illustrated in Fig. 2. It demonstrates the way how to make the current in a magnetic diode larger or smaller. Referring Fig.2 below, if we look at the potential barrier going from the n- to p-region, we see that by making the spin in the n-region non-equilibrium, pointing-up electrons, will have a lower barrier to cross, increasing the recombination current. On the other hand, introducing more spin-down electrons in the n-region, electrons have to climb a higher barrier, reducing the recombination current. Since the generation current is not influenced by the non-equilibrium properties, the current for the parallel orientation will be larger than that for an antiparallel orientation of the equilibrium and non-equilibrium spins [8].

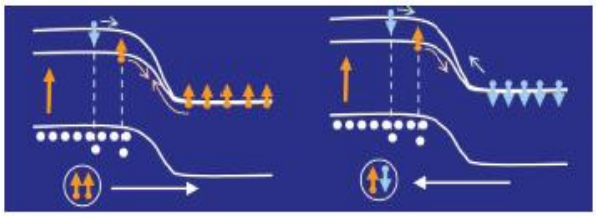

Fig. 2. Spin-voltaic effect in a magnetic diode [8].

iii). Conventional Bipolar Junction Transistor: In a conventional transistor, say n-p-n type, when a voltage is placed across the gate, free electrons either are attracted towards the gate (base) or away from it, depending on the direction of the applied voltage. This lack or presence of gate electrons controls the flow of current between emitter and collector, allowing the transistor to occupy ON or OFF states [9].

The problem with conventional transistors is their volatility. When power is shut off, the electrons in the p-type semiconductor are no longer confined to a single region and diffuse throughout, destroying their previous ON or OFF configuration. This volatile effect can be avoided by introducing, a new type of transistor known as magnetic transistor [9].

iv). Magnetic bipolar transistor:

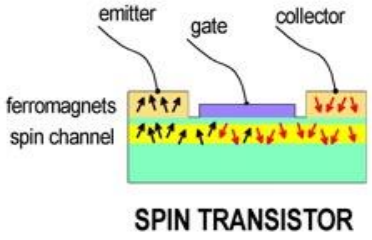

Fig 3. Magnetic Transistor.

In a magnetic transistor Fig. 3, magnetized ferromagnetic layers replace the role of n and p-type semiconductors. As in a conventional field effect transistor there is a third electrode (gate) that generates an electric field to modulate the current in the transport channel. The magnetizations of injector and detector are assumed to be parallel [10]. In case of zero gate voltage, every electron emitted from the injector with its spin oriented along the magnetization direction enters the detector with no change to spins during transport. For nonzero gate voltage the gate electrode produces an electric field that causes the spins to process. Substantial current can flow through parallel magnetized ferromagnetic layers. However, if, say, in a three layer structure, the middle layer is antiparallel to the two outside layers, the current flow would be quite restricted, resulting in a high overall resistance.

PARAMETRIC INVESTIGATION AND SURVEY OF CURRENT SENSORS

Current sensors are electrical devices which measure currents in a cable or a wire and generate a signal of some sort in response to the current. In most electrical device current monitoring is more meaningful compared to voltage monitoring because current signal contain much valuable information such as harmonics, unbalanced load in electric power distribution systems, unbalanced forces and motor / bearing irregularities in motor drive train traction system. In addition to this, current sensors are widely used as feedback devices in field industrial equipment, power system protection, and various test-controlled systems [11].

We may classify current sensors as the conventional current sensors and spintronics current sensors. The conventional current sensors include traditional current transformers, resistive shunt, Rogowski current sensors, fluxgate current sensors, and Hall effect current sensors. And the spintronics current sensors include: AMR (Anizotropic Magneto-Resistnce) current sensors, and GMR (Giant Magneto-Resistance) current sensors or (spin valve current sensors) [12][13] .

Sensor parameters

Sensor's parameters characterize its performance as a sensor. The performance of the current sensors consists of static, dynamic and thermal characteristics, and determines its application. The static characteristics include the sensor's range, sensitivity, offset voltage, linearity and accuracy while a dynamic characteristic consists of the frequency response of the sensor, the amplitude response and the phase response of the sensors. Since sensitivity is the most important figure of merit for all sensors the paper considers only this performance parameter.

In this work, sensitivity is understood as, the smallest absolute amount of change that can be detected by a measurement.

Parametric investigation of Electronics current Sensors

Hall Effect integrated circuits are used in a wide range of applications, like in computers, automobiles, aircraft, and medical equipment etc. It is possible to construct high-quality Hall-effect transducers with the standard integrated circuit processes and by integrating it to auxiliary signal-processing circuitry, on the same silicon die; usable sensors can be fabricated [14]. Because of the above reasons, among different electronics current sensors, we focus and investigate the researches done on Hall Effect current sensors.

In the first survey we see the research which aims to prove the combined Hall sensors and coils to obtain a wideband, CMOS-compatible, contactless current sensor. This study fabricated orthogonally-coupled normal n-well; normal n-well with 45° orientation; p+ doping pinched n-well and poly gate covered n-well Hall sensor

Table 1 Summarized electronics current sensor investigation table

survey	**Material used**	**Result**	
		Sensitivity	
		A	*B*
Survey-1 [20]	p-substrate, N-well implantation and p+ doping	113.13 V/AT	116.94 V/AT
		115.27 V/AT	119.51 V/AT
		113.63 V/AT	117.65 V/AT
		115.42 V/AT	119.53 V/AT
		108.36 V/AT	114.07 V/AT
		117.24 V/AT	121.14 V/AT
		114.15 V/AT	117.95 V/AT
		113.40 V/AT	118.04 V/AT
Survey-2 [22]	p-substrate, N-well implantation and p+ diffusion	80.7 V/AT	
Survey-3 [23]	N-type Epi Resistance (InGaAs/InP: Si[100]), P-type Well Resistor, P+ Resistor	19.9 uV/G/single hall plate/Ceramic package/160µm	
		17.1 uV/G/single hall plate/plastic package/160µm	
		19.6 uV/G/Quad hall plate/ceramic package/160µm	
		17.0 uV/G/Quad hall plate/plastic package/160µm	
		18.3 uV/G/single hall plate/Ceramic package/50µm	
		15.6 uV/G/single hall plate/plastic package/50µm	
		15.4 uV/G/Quad hall plate/ceramic package/50µm	
		19.9 uV/G/quad hall plate/plastic package/50µm	
Survey-4 [21]	substrate δ-doped GaAs, 6000Å Buffer δ -doped GaAs, 120Å Channel δ -doped $In_{0.18}Ga_{0.82}As$, 50Å Spacer δ -doped $Al_{0.35}Ga_{0.65}As$, 200Å supply $Al_{0.35}Ga_{0.65}As$ and 50Å Cap GaAs	8 mV/mT	

	substrate δ-doped GaAs, 6000Å Buffer δ-doped GaAs,Channel δ-doped $In_{0.15}Ga_{0.85}As$, Spacer δ-doped 50 Å $Al_XGa_{(1-X)}As$, supply $Al_XGa_{(1-X)}As$ and 100Å Cap GaAs	16 V/μT

prototypes. As the result different values of sensitivity are obtained in each prototype in different sizes

The research of the second survey targets to investigate the effect of sensitivity of the Hall Effect current sensor with biasing current and temperature. The result of the research declares sensitivity to have linear relation with biased current and temperature. The third survey assesses the research which focuses on the effect of stress on the sensitivity. This research utilizes two 160μm and 50μm side length Hall plates with one quad Hall plate, and with two single Hall plates in each size encapsulated in plastic and ceramic packages. As a result different values of sensitivity are obtained. The research discussed in the fourth survey focused on the way of avoiding offset and noise, improve sensitivity and reduce the power conception of the Hall Effect current sensor. The research design is categorized in to DC and AC Linier Hall Effect sensors and obtains two improved sensitivity results as compared to the other similar types of current sensors.

Spintronics current Sensor

The whole GMR effect sensor system contains three main subsystems: The sensing head which is used to convert the measured current signal to the voltage signal. The signal processing subsystem which helps to process the voltage signals of the sensing head output and calculate the measured current. The power supply subsystem to provide the power source for the whole sensor system. In the design of the GMR chip, in order to convert the magnetic signal to a voltage signal, four identical spin-valve resistors making up a Wheatstone bridge are used Fig. 4. In the bridge circuits two of the resistors are sensing resistors; the other two are reference (Shield) resistors.

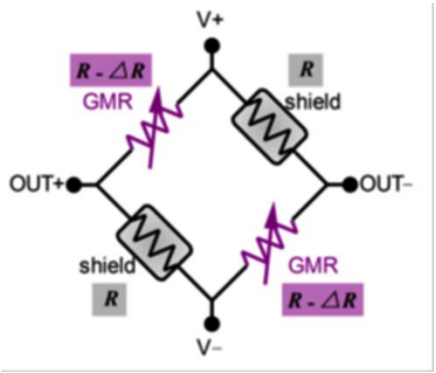

Fig. 4. Wheatstone bridge of GMR chip [15].

Parametric investigation of Spintronics current Sensors

In this section, the research on a Spintronics current sensors based on GMR effect are investigated. As per the investigation, it is found that, the performance parameters of the current sensor varies depending on the material, the size and the number of magneto-resistive elements used per bridge resistor.

In the first survey the research under investigation uses serial and parallel configurations with 10 cm and 100 μm width of the current strap respectively. The result shows that the sensitivity in both cases is similar; however the power consumption is found different. The study of the second survey presents three different configurations, with one, three, and seven magneto-resistive elements per bridge resistor. The study obtains three different sensitivity results which are relatively close to each other and it concludes that sensitivity doesn't improve much with increasing impedance. In the third survey the assessed research studied the feasibility of spin-valve sensors when working in high-frequency power electronics applications. As a result it is reported that with application of as large current as, (up to 10A) good sensitivity is observed, but the accuracy obtained is degraded. In the fourth survey uncoupled hard and soft-magnetic layers are used, and field is applied repeatedly, and the study shows the sensor performance is affected strongly at the beginning; indeed no further change observed. The summarized results of the researches are presented in the table below.(Table 2)

RESULT COMPARISON

Each of the above summarized sensitivity data of spintronics and conventional electronics current sensors have different units. To simplify the comparison it needs to change in to identical unit of measurement.

For example, in the electronics current sensors first survey, the value of sensitivity of the first sample under category A is

$113.13\frac{V}{AT}$. To convert in to $\frac{V}{T}$ we should multiply by the 2A DC biased current used during sensitivity measurements.

Therefore:

$$113.13\left(\frac{V}{AT}\right)\times 2A = 226.26\left(\frac{V}{T}\right)$$

If we take sample S_1 of the second survey of spintronics current sensors the sensitivity value is $0.86\frac{mV}{VmA}$ at 1mA biased current per 20 (Oe) of magnetizing field using 5mV.

Table 2 Summarized spintronics current sensor investigation table

survey	Sensor code	Material used	Sensitivity Result
Survey-1 [16]	SV07-SN (10cm)	Si / SiO2 (1500Å) Substrate; Ta (20 Å) Buffer; NiFe (30 Å) and CoFe (20 Å) Free layer; Cu (22 Å) Separator; CoFe (20 Å) Pinned layer; MnIr (60 Å) Ferromagnetic/ Antiferromagnetic layer and Ta (40 Å) Passivation Layer	< 0.5 nTesla/√HZ or < 1 Oe/mA
	SV07-PW (100µm)		< 0.5 nTesla/√HZ or < 1 Oe/mA
urvey-2 [17]	S-1	Si / SiO2 (1500Å) Substrate; Ta (20 Å) Buffer; NiFe (30 Å) and CoFe (20 Å) Free layer; Cu (22 Å) Separator; CoFe (20 Å) Pinned layer; MnIr (60 Å) Ferromagnetic/ Antiferromagnetic layer and Ta (40 Å) Passivation Layer	0.86 forDC, 0.87 ±0.1 for AC) mV/(V mA)
	S-2		**0**.81 forDC, 0.87 ±0.1 for AC) mV/(V mA)
	S-3		0.79 forDC, 0.87 ±0.1 for AC) mV/(V mA)
Survey-3 [18]	-	Si / SiO2 (1500Å) Substrate; Ta (20 Å) Buffer; NiFe (30 Å) and CoFe (20 Å) Free layer; Cu (22 Å) Separator; CoFe (20 Å) Pinned layer; MnIr (60 Å) Ferromagnetic/ Antiferromagnetic layer and Ta (40 Å) Passivation Layer	0.91 mV/ (V.Oe)
Survey-4 [19]	-	Si Substrate; Fe Buffer; CoFe Free layer; Cu (> 2 nm) Separator; CoFe Pinned layer; Co_x $Cu_{1\ nm}Co_y$ $Cu_{1\ nm}Co_x$ Ferromagnetic/ Antiferromagnetic layer and Fe Passivation Layer	2 mV V^{-1} (kA m^{-1})$^{-1}$

where (Oe --- in Ampere /Meter) known as Oersted, is a magnetic field strength unit.

Now to convert in to $\frac{V}{T}$

$$0.86\left(\frac{mV}{VmA}\right)\times 1mA = 0.86\left(\frac{mV}{V}\right)$$

Dividing by the field

$$\frac{0.86\frac{mV}{V}}{20(Oe)} = 0.043\left(\frac{\text{mV}}{\text{V (Oe)}}\right)$$

$$1\ (Oe) = \frac{10^3}{4\pi}\left(\frac{A}{m}\right)$$

And

$1G = \frac{10^3 A}{m}$, where G is - Gauss

Therefore

$$1(Oe) = \frac{1}{4\pi}G$$

Also

$$1G = 10^{-4}T$$

So

$$1(Oe) = \frac{10^{-4}}{4\pi}T$$

$$\left(\frac{0.043}{\frac{10^{-4}}{4\pi}}\right)\frac{\text{mV}}{\text{VT}}$$

$$\left(\left(\frac{0.540}{10^{-4}}\right)\times((10^{-3})\right)\left(\frac{V}{VT}\right) = 5.40\frac{V}{VT}$$

Multiplying by the used voltage amount, we obtain

$$\left(5.40\left(\frac{V}{VT}\right)\right)\times\left((5\times 10^{-3})V\right) = 0.027\left(\frac{V}{T}\right)$$

All other data units are converted in similar fashion, but depending upon the units, the way of conversion and the units used for conversion may be different. The converted results are presented in the table below. Table 3 Result comparison table

Sensor Technology	Sensitivity(V/T)	Range of sensitivity (V/T)
Electronics Current Sensor (Hall Effect)	226.26	(0.154-242.28)
	233.880	
	230.540	
	239.020	
	227.260	
	235.300	
	230.840	
	239.060	
	216.720	
	228.140	
	234.480	
	242.280	
	229.000	
	235.900	
	226.800	
	236.080	
	0.560	
	0.199	
	0.171	
	0.196	
	0.170	
	0.183	
	0.156	
	0.154	
	0.199	
	8.000	
Spintronics Current Sensor (spin Valve)	0.027	(0.004-3.431)
	0.127	
	0.049	
	0.136	
	3.431	
	0.004	

We notice that sensitivity is defined as the smallest absolute amount of change that can be detected by a measurement. The result obtained from the sensitivity study is presented in the form of table and graphs. As we see from the table III above the range of the sensitivity of the spintronics sensor is 0.004 to 3.431 Volts per Tesla, while the range of sensitivity of the electronics sensor is 0.154 to 242.28 Volts per Tesla. Fig. 5 and Fig.6 show the smallest, the average, and the largest sensitivity values of both electronics and spintronics current sensors using line graph, and bar graph respectively. From both graphs we can observe that, the sensitivity of spintronics current sensors is in a very low range than electronics current sensor. For further clarification, Fig. 7 presents the comparison of the smallest sensitivity values of both spintronics and electronics current sensor in the form of bar graph.

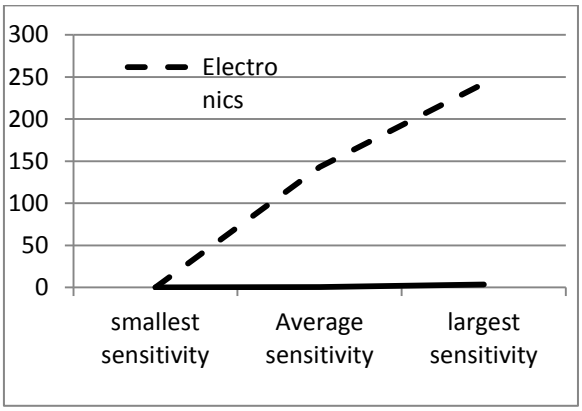

Fig. 5. Smallest, Largest and Average sensitivity of spintronics Vs Electronics current sensor in line graph

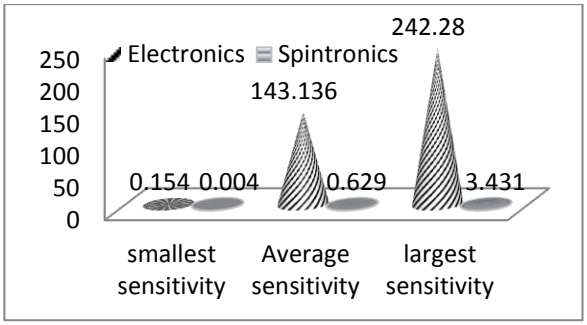

Fig. 6. Smallest, Largest and Average sensitivity of spintronics Vs Electronics current sensor in bar graph

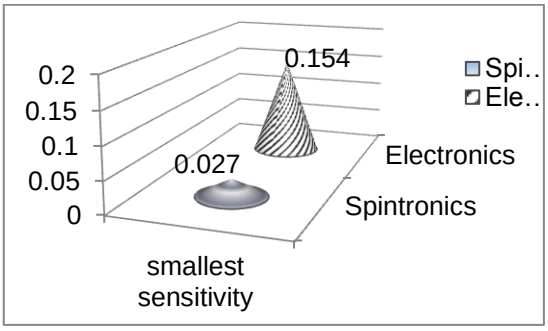

Fig. 7. The Smallest sensitivity of spintronics Vs Electronics current sensor in bar graph

CONCLUSION

In this paper, the working principle of spintronics devises in relation to the conventional electronics devises is discussed. Survey of research works on electronic sensors with different configurations is made and also survey of researches on spintronics based sensors with different configuration is done each separately.

Based on the sensitivity parameter of the sensors, the researches done by the two different schools is investigated and compared. The results of comparison are demonstrated by tables and graphs. Based on the survey we did, and from the comparison results we observed we conclude that the spintronics current sensors are highly sensitive and more applicable than the conventional electronics current sensors.

REFERENCES

[1] Shailendra Kumar Singh, " Spintronics Technology", Department of Electronics and Communication Engg, University College of Engineering, Rajasthan Technical University, Kota, A Seminar Report, 2010-2011

[2] Igor Z ˇ utic, Jaroslav Fabian, S. Das Sarma, "Spintronics: Fundamentals and applications", Reviews of Modern Physics, Volume 76, April 2004

[3] Teruya Shinjo, "Nano Magnetism and spintronics", 2009

[4] R.A. Duine, "Spintronics", Institute for Theoretical Physics, Utrecht University, Netherlands, February 24, 2010

[5] David D. Awschalom, Ryan Epstein and Ronald Hanson,"The Diamond Age of spintronics", October 2007

[6] Volodymyr Karpan, "Spintronics: A First-Principles Study", University of Twente, September 1977

[7] Hyunsoo Yang, "Metal Spintronics: Tunneling Spectroscopy Injunctions with Magnetic and Superconducting Electrodes" March 2006

[8] Jaroslav Fabian, Alex Matos-Abiaguea, Christian Ertlera, Peter Stano, Igor Z˘utic´ "Semiconductor Spintronics''

[9] Micro Magnetics, Inc. "What is Spintronics? a.k.a Magnetoelectronics, Spin Electronics, or Spin-based Electronics"

[10] Volodymyr Karpan, "Spintronics: A First-Principles Study", University of Twente, September 1977

[11] Kaj Iwansson, GiJnther Sinapius, Winfried Hoornaert; "Handbook Of Sensors and Actuators, Measuring Current Voltage and Power"; ELSEVIER; 1999

[12] Farzad Nasirpouri, "Nanomagnetism and Spintronics Fabrication, Materials, Characterization and Applications", Sahand University of Technology, Iran Alain Nogaret University of Bath, UK 2009

[13] Yong Ouyang , Jinliang He, Jun Hu and Shan X. Wang; "A Current Sensor Based on the Giant Magnetoresistance Effect: Design and Potential Smart Grid Applications"; 2012.

[14] Edward Ramsden "Hall-Effect Sensors Theory and Application"; Newnes; 2006 ; Sensors

[15] R S Popovic; "Hall Effect Devices"; Second Edition; Swiss Federal Institute of Technology Lausanne (EPFL); 2004

[16] A. Roldan, C. R., M.D. Cubells-Beltran, J.B. Roldan, D. Ramirez, S. Cardoso, P.P. Freitas (2010). "Analytical compact modeling of GMR based current sensors: Application to power measurement at the IC level." Solid-State Electronics elsevier.

[17] C. Reig, D. R. ı., F. Silva, J. Bernardo, and P. P. Freitas (June 2004). "Spin-valve current sensor for industrial applications"; Science Direct Elsevier B.V.

[18] Diego Ramírez Muñoz José Pelegrí Sebastiá, Paulo Jorge Peixeiro de Freitas, and Wanjun Ku, "A Novel Spin-Valve Bridge Sensor for Current Sensing'"; IEEE Transactions On Instrumentation And Measurement Vol. 53; June 2004

[19] Michael Vieth, Wolfgang Clemens, Hugo van den Berg, Gu¨nter Rupp, Joachim Wecker, Matthias Kroeker ; "Contactless current detection with GMR sensors based on an artificial antiferromagnet _AAF/ subsystem"; Elsevier Science, Sensors and Actuators volume 81;2000

[20] Junfeng Jiang;" Design of a Wide-Bandwidth Magnetic Field Sensor"; Delft University of Technology, Faculty of Electrical Engineering, Mathematics and Computer Science ; September 2011

[21] Mohammadreza Sadeghi;"Highly Sensitive Nano Tesla Quantum Well Hall Effect Integrated Circuits using GaAs-InGaAs-AlGaAs 2DEG"; University of Manchester faculty of Engineering and Physical Sciences; February 2015

[22] Maria-Alexandra Paun, Jean-Michel Sallese, Maher Kayal; "Temperature considerations on Hall Effect sensors current-related sensitivity behavior"; 15 October 2013

[23] Juan Manuel Cesaretti; "Mechanical Stress and Stress Compensation"; Georgia Institute of Technology; May 2008

STUDY ON POWER DISTRIBUTION NETWORK AUTOMATION TO MITIGATE POWER OUTAGES

*Dawit Habtu Gebremeskel, and Getachew Biru Worku,
School of Electrical and Computer Engineering,
Addis Ababa Institute of Technology, Addis Ababa University
*Corresponding Author's E-mail: dawit.habtu@aait.edu.et

ABSTRACT

The paper presents development of an appropriate distribution system automation to mitigate power outages and improve reliability of the system. Addis Ababa distribution system is taken as a case study to demonstrate the effectiveness of the proposed technique. It is found that 55% of the number of interruptions and 46% of the total duration of interruptions in the existing Addis Ababa distribution system are due to distribution system related problems. The proposed distribution system automation is capable of detecting feeder faults, determining the fault location, isolating the faulty section of the feeder and finally restoring power supply to healthy portions of the feeder. Thus, it has the capacity to significantly improve the reliability of the distribution system.

The performance of the designed model is evaluated through simulation studies to check the reliability improvement of Addis Ababa distribution network. The simulation results show that the System Average Interruption Duration Index (SAIDI) and System Average Interruption Frequency Index (SAIFI) is improved by 69% and 88%, respectively. Thus, it is observed that the frequent interruptions and outages in the existing Addis Ababa distribution system could be potentially mitigated by implementing the proposed automation of Addis Ababa distribution network.

Key Words: Distribution Automation, Distribution Network, Medium Voltage Line, Interruption, Power Outage, Reliability.

INTRODUCTION

Electric power distribution system is an important part of electrical power systems that determines supply reliability or proper delivery of electricity to consumers.

Generally speaking, customer expectations on supply reliability are steadily increasing [1]. The owners of distribution network are being required to improve the reliability of power delivery through making the whole operating condition more efficient. In some cases, explicit power quality criteria are even included in negotiated contracts between customers and utilities[1]. Moreover, in liberalized markets, regulators typically require the utilities to report on the reliability performance or even penalize them in case of violations in several countries [2].

Distribution Automation (DA) is the remote control of switches to locate, isolate faults and restore the service, when a fault occurs in the power distribution line. It also results into a highly reliable, self-healing power system that responds rapidly to real-time events with appropriate actions [3, 4]. This concept combines the ability to mix local automation, remote control of switching devices, and central decision making into a cohesive, flexible, and cost-effective operating architecture for power distribution systems[5].

Automation in the distribution field allows utilities to implement flexible control of distribution systems, which can be used to enhance efficiency, reliability and quality of electric service [1,3,6]. From the analysis of Recloses and Sectionalizers, it is found that there is a significant improvement in the reliability of a distribution feeder and as a result, coordinated system of these devices can significantly improve the reliability indices SAIDI and SAIFI[1,6].

The successful implementation of DA system results mainly in Operational & Maintenance benefits, financial benefits, and customer related benefits[3]. These benefits are related to the improved reliability, reduced operation and maintenance expenses, reduced fault location time, increased revenue due to quick restoration, reduction in staffing, enhanced system efficiencies and consumer satisfaction.

The above cited researches clearly reveal the importance of the technology in addressing mainly, reliability and efficiency issues for the specified distribution networks, but before deciding to go ahead with the technology, the potential drawbacks, interruption causes, power outage levels and shortcomings of the old system should be studied in detail. Then, it should be verified that these identified problems could be mitigated by deploying DA for that specific utility company or distribution network. The aim of this research is, therefore, to develop an appropriate distribution automation model that can potentially mitigate the power outages occurring on the existing Addis Ababa distribution system.

Case Study: Present State of Addis Ababa Distribution Network

Power distribution network in Addis Ababa is effected at a primary voltage of 33 and 15kV consisting entirely of 3-phases, 3-wire feeders and is stepped down to a utilization voltage of 380/220V (3-phase, 4 wire) and 500V for some industries using 3-phase transformers to customer's level. The distribution system in Addis Ababa consists of 32,373.39 km of 33kV and 15kV; 95,000km of 380/220V lines and 6,339 distribution transformers[3]. Even though, there are many efforts and launched projects to modernize Addis Ababa's underground electric cable installation, the medium voltage (MV) and Low Voltage (LV) networks are still dominated by overhead lines.

In the radial distribution network structure of Addis Ababa, there are manually controlled three phase switches (MCOS) or section switches located on the beginning of each branch circuit that can interrupt the supply for planned outages like maintenance or unplanned outages of various disturbances. But, the network is not suited with additional equipments such as remote controlled switches, automatic reclosers, sectionalizes, remotely controlled fault passage indicators, etc. which would contribute a lot in improving the overall reliability. In a radial distribution system, only one path is connected between each customer and the substations. i.e. The electrical power flows from the substation to the customer along a single path which if interrupted results in complete loss of power to the customer. Such system has only one power source for a group of customers and is usually suitable for sparsely populated areas. For a city like Addis Ababa, with a population density of 5,165.1/km^2 and with a huge power demand such kind of network configuration is unsuccessful and that was exactly what has been witnessed for the past years. On top of this, the whole system can only be operated manually which makes it difficult to monitor the system state as well as to take any action.

Knowing this, Ethiopian Electric Utility, EEU (formerly known as Ethiopian Electric Power Corporation, EEPCo) planned to modify the system to a ring system by installing several switching stations in between various substations [7]. However, only few of the total number of feeders per substation, which are believed to encounter many faults, have been made to interconnect to other substations.

In the existing distribution system, pinpointing the exact or even approximate location of faults is difficult, even though fault passage indicators are installed in various switching stations. Dispatchers still depend on telephone calls from customers and substation Operators. Customers' calls only provide an approximate location of the outage. Once the approximate location of outages is known, line crews are dispatched to drive along the lines to look for damage. After the damaged area is located, it has to be isolated from the rest of the system if the fuse protecting that line has not operated. This is done by first opening the substation breaker and then manually operating the switches or removing the fuses. Coordination between the line crews and dispatchers is maintained via portable radio to perform this task properly or via mobile telephone. The next step is to restore power to those parts of the system which are undamaged but have lost power because of problems elsewhere in the system. The power to these parts may be provided from alternates routes. The dispatchers determine such possible routes and ask the line crew to operate the isolators. Most of the isolators cannot be operated under load; therefore, the substation breaker is opened before operating the isolators. Since the whole process is done manually, it takes a long time. This is depicted in figs. 1 and 2. Automation of this function requires installation of devices such as reclosers, remotely controlled Sectionalizers and installation of sensors on the feeders and/or at customer locations to detect interruption of service.

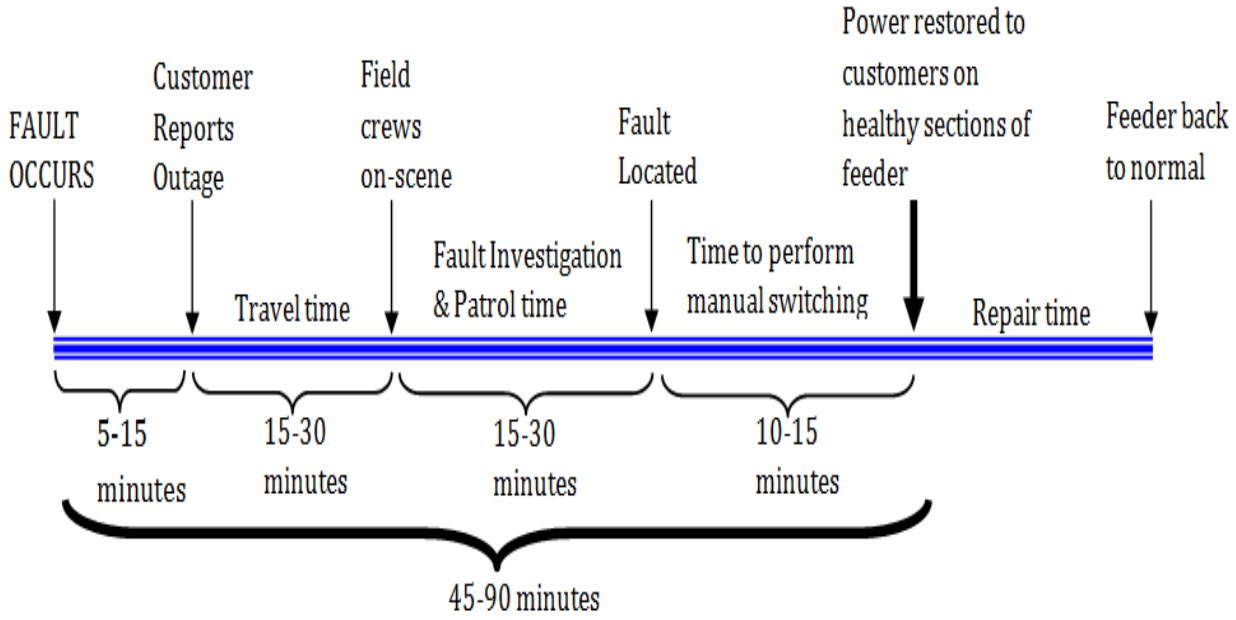

Fig. 1: Activity-time diagram for a permanent feeder fault without automation

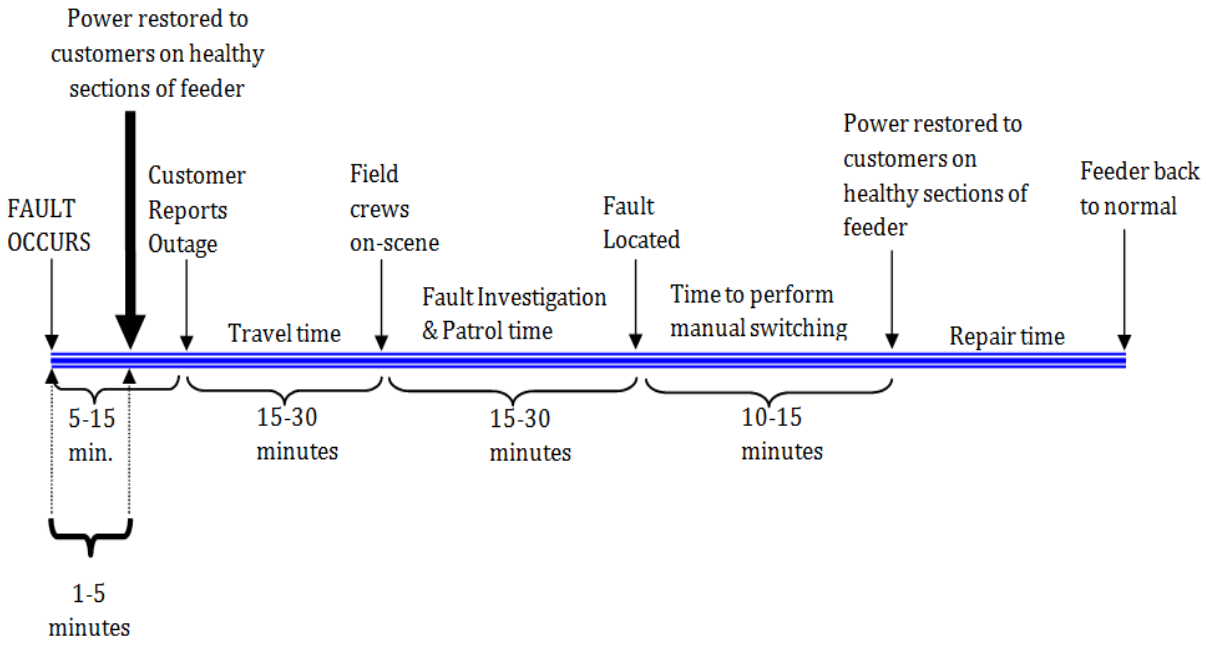

Fig. 2: Activity-time diagram for a permanent feeder fault with proposed automation model

Reclosers

A recloser is a device with the ability to detect phase and phase-to-ground overcurrent conditions, to interrupt the circuit if the overcurrent persists after a predetermined time, and then to automatically reclose to re-energize the line. If the fault that originated the operation still exists, then the recloser will stay open after a preset number of operations, thus isolating the faulted section from the rest of the system. Thus, the recloser, with its opening/closing characteristic, prevents a distribution circuit being left out of service for temporary faults.

Reclosers are used at the following points on a distribution network:

- In substations, to provide primary protection for a circuit,
- In main feeder circuits, in order to permit the sectioning of long lines and thus prevent the loss of a complete circuit due to a fault towards the end of the circuit,

- In branches, to prevent the tripping of the main circuit due to faults on the spurs.

Sectionalizers

A sectionalizer is a device that automatically isolates faulted sections of a distribution circuit once an upstream breaker or recloser has interrupted the fault current and is usually installed downstream of a recloser. Since sectionalizers have no capacity to break fault current, they must be used with a back-up device that has fault current breaking capacity. Sectionalizers count the number of operations of the recloser during fault conditions. After a preselected number of recloser openings, and while the recloser is open, the sectionalizer opens and isolates the faulty section of the line.
Therefore, the switching needed to restore power to unfaulted parts of the system can be accomplished remotely. Moreover, since the location of the outage is known, the crew is sent to the precise location instead of asking to go in a general area. Thus, the whole process of outage location and service restoration can be accomplished more efficiently by less people in much less time.

Power interruptions in the Existing Addis Ababa Distribution System

The frequency and duration of interruptions occurring on the different feeders of Addis Ababa distribution system are given in Table 1 and plotted in figs. 3 and fig. 4, respectively. The system average interruption duration index (SAIDI) and system average interruption frequency index (SAIFI) are calculated as discussed below and are listed in Table 3.

a) System Average Interruption Duration Index (SAIDI)

This index measures the total duration of an interruption for the average customer during a given time period. To calculate SAIDI, each interruption during the time period is multiplied by the duration of the interruption to find the customer-hrs/mins of interruption. The customer-hrs/mins of all interruptions are then summed to determine the total customer-hrs/mins. To find the SAIDI value, the customer-hrs are divided by the total customers served.
The formula is,

$$SAIDI = \frac{\sum(r_i \times N_i)}{N_T}$$

Where,
r_i=Restoration time (hrs./mins.)
N_i=Total number of customers interrupted
N_T=Total number of customers served

b) System Average Interruption Frequency Index (SAIFI)

The System Average Interruption Frequency Index (SAIFI) is the average number of times that a system customer experiences an outage during the year or time under study. The SAIFI is found by dividing the total number of customers interrupted by the total number of customers served.
SAIFI is found as:

$$SAIFI = \frac{\sum(N_i)}{N_T}$$

Where,
N_i=Total number of customers interrupted
N_T=Total number of customers served

From table 1, it can be seen that the annual SAIDI is about 209 Hrs., which means that on the average each customer in Addis Ababa was without power supply for 209 Hrs. due to interruptions on MV- feeders during that year. It can also be seen that the annual SAIFI is about 184, indicating power for each customer in Addis Ababa has been interrupted on the average 184 times in a year. According to the reliability standard set by Ethiopian Energy Authority (formerly known as Ethiopian Electricity Agency)[8], these reliability indices clearly illustrate that the reliability of the power network is very poor.

Causes of Interruptions

The faults in the electricity network may have various forms as illustrated in table 2. These faults could be mainly of two types, namely, transient (temporary) and permanent faults. Usually, transient faults occur when phase conductors electrically contact other phase conductors or ground momentarily due to trees, birds or other animals, high winds, lightning, flashovers, and so on. Transient faults are cleared by a service interruption of sufficient length of time to extinguish the power arc or electric discharge. Here, the fault duration is minimized and unnecessary fuse blowing is prevented by using instantaneous or high-speed tripping and automatic reclosing of a relay-controlled power circuit breaker or the

automatic tripping and reclosing of a circuit recloser [9].

The breaker speed, relay settings and recloser characteristics are selected in a manner to interrupt the fault current before a series fuse is blown, which would cause the transient fault to become permanent. Permanent faults are those which require repairs by repair crew in terms of [9]:

- Replacing burned-down conductors, blown fuses, or any other damaged apparatus
- Removing tree limbs from the line
- Manually reclosing a circuit breaker or recloser to restore service

From Fig. 5 pie chart plot, it can be seen that, 55% of the total number of power interruptions are due to distribution related problems such as Distribution Permanent Earth Fault (DPEF), Distribution Permanent Short Circuit (DPSC), Distribution Transient Earth Fault (DTEF), Distribution Transient Short Circuit (DTSC), Distribution Line Over Load (DLOL) and the rest 45% are due to others like generation, transmission problems and operational or intentional isolation.

Fig. 6 pie chart plot shows the duration of interruption in Addis Ababa based on specific fault type. Similarly, it can be seen that 45.92% of the total duration of interruptions are due to distribution related problems and the rest 54.08% are due to others as mentioned above. The above percentage figures clearly demonstrate that distribution related problems account significant share for the cause of the interruptions which can be improved by employing appropriate mitigating technology.

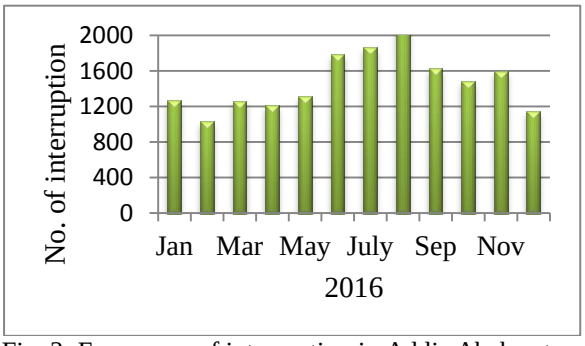

Fig. 3: Frequency of interruption in Addis Ababa at feeder level, (Source: EEU)

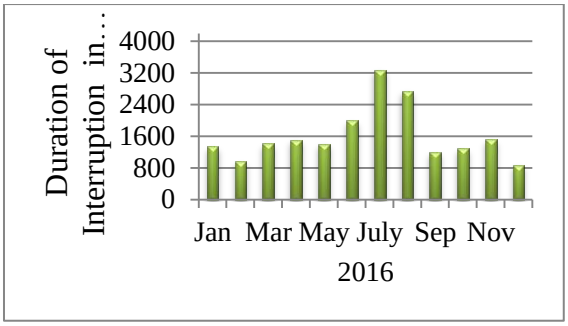

Fig. 4: Duration of interruption in Addis Ababa at feeder level, (Source: EEU)

Overview of Proposed Automated Feeder System

Fig. 7 demonstrates the proposed model for the automated feeder system to detect feeder faults, determine the fault location, isolate the faulted section of the feeder and finally restore service to healthy portions of the feeder.

The local scheme involves detection, location of the fault and isolation of the affected area through various field components. Whereas, the centralized scheme which involves the central station is needed to monitor and restore the service of the feeder system.

The main components to be needed for the feeder automation are protection relay (R), automatic reclose (RC), sectionalized (S) and tie switches (Tie) or load break switch. The number of sectionalizes considered in this model are four, but it may vary depending on the total length of the feeder and loading level in each section.

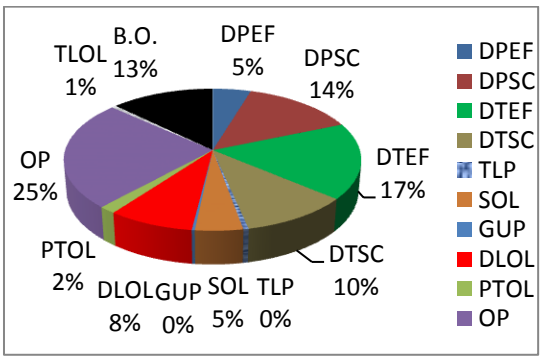

Fig. 5: Average percentage of Frequency of interruption

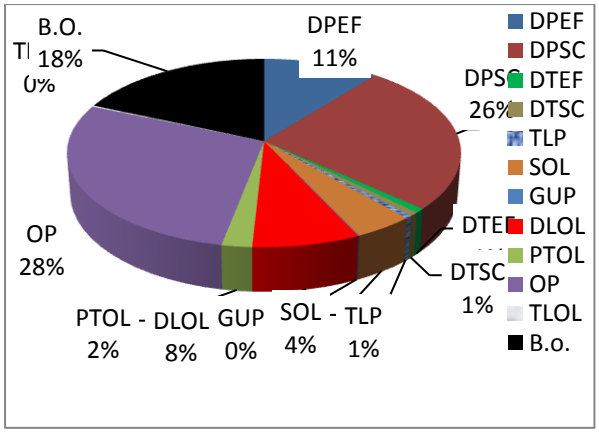

Fig. 6: Average percentage of Duration of interruption for feeders in Addis Ababa based on fault type.

In the model, three medium voltage lines or outgoing feeders from the same substation or neighboring substations are considered for interconnection, so that, it is possible to restore the service to the healthy sections of the contingent feeder from either of the remaining two routes by taking their loading into consideration. i.e. The operator checks which feeder is strong enough to carry the additional load and closes the respective tie switch to restore the service to the healthy section of the contingent feeder. When a transient fault occurs at any of the sections, the assigned/responsible recloser will try to reclose the circuit automatically and restores the feeder to its normal condition. If a permanent fault occurs in either of the sections, the recloser will lock out after its third trial and the fault detectors which employ fault location algorithm by taking the network structure information and obtained measurements of fault currents and voltages as input located at each of the sectionalizers will detect the fault, report and give flash. Then, the nearby sectionalizers surrounding the fault will automatically open which makes the faulted section to be isolated. After that, the operator closes the circuit breaker and simultaneously checks whether the alternate feeder can carry the additional load (downstream to the isolated section) of the faulty feeder. Finally, the operator will remotely close the respective tie switch which will supply the disconnected load until the permanent fault is cleared. All of the above activities including the coordination of the protective and isolation devices are discussed in detail in the next sections.

SIMULATION RESULTS AND ANALYSIS

The protection scheme of a 15kV distribution feeder feeding loads at different sections is done with Tavrida Electric Automated Relay Manager (TELARM) software tool as shown in fig. 8. Only four sections are considered for the ease of demonstration and the same principle can be applied to any number of sections whenever needed. It is assumed that the recloser will lockout after 4 number of trips with reclosing times 1, 5, 10 and 60 sec. for first, second, third and reset reclosings respectively. Sectionalizers S1, S2 and S3 are set at 3, 2 and 1 shot respectively. If the autorecloser trips the fourth time (after the third reclosing shot), the fault is regarded as permanent. Hence, further autorecloser operation is locked out. During the process of auto reclosing, various sections would be removed out of the line with the help of sectionalizers to power the healthy portion of the feeder. If the fault is permanent in nature, then the automation control unit can intervene to restore the service to healthy sections from other alternative feeders by sending remote switching commands to sectionalizers.The cycle of switching of the different reclosers and sectionalizers is described during this time as follows. Fig. 9 presents the state of the reclosers and sectionalizers under permanent fault at section 3 (between S2 and S3) by using different colors where green represents closed state, violet represents open state, yellow represents reclose time, blue represents tripping time and red represents open and lockout state. Primarily, R performs the first reclosing cycle and trips again as presented above. Then, R times out for 5 seconds and S3 trips and locks out. Then, R closes for a second time. S2 and S1 sense the control voltage and close the first time. A fault current passes through R and R trips for the third time and times out for 10 seconds. At this point, the control voltage is lost and S2 trips the second time and locks out. Finally, R closes for the third time and the fault on section 03 is isolated. The Operator in control unit will try to remotely close S2 and S3 after clearance of the permanent fault. Similarly, all transient and permanent faults are created at various sections of the feeder for demonstrating the responses of the various switching and protection devices installed throughout the feeder.

Table 1: Frequency and duration of interruption in Addis Ababa at all feeders, (Source: EEU)

No.	Period	Frequency of Interruption (No.)	Duration of Interruption (Hr.)	SAIDI Values (hrs./customer)	SAIFI Values (no./customer)
1.	Jan, 2016	1,265	1,348.58	13.50	12.39
2.	Feb, 2016	1,029	953.88	9.35	10.64
3.	Mar, 2016	1,260	1,413.15	14.26	12.42
4.	Apr, 2016	1,210	1,507.03	19.22	12.10
5.	May, 2016	1,308	1,402.55	14.12	14.94
6.	June, 2016	1,781	2,001.22	22.96	18.02
7.	July, 2016	1,864	3,280.00	34.50	19.06
8.	Aug, 2016	2,363	2,742.00	28.49	22.36
9.	Sep, 2016	1,628	1,208.00	11.89	17.96
10.	Oct, 2016	1,483	1,290.00	11.95	15.32
11.	Nov, 2016	1,596	1,527.00	19.87	17.15
12.	Dec, 2016	1,145	872.00	8.85	11.31
Total (year 2016)		17,932	19,545.61	209	184

Table 2: Acronyms and Description of Faults System

Fault Acronym	Fault Type
DPEF	Distribution Permanent Earth Fault
DPSC	Distribution Permanent Short Circuit
DTEF	Distribution Transient Earth Circuit
DTSC	Distribution Transient Short Circuit
TLP	Transmission Line Problem
SOL	System Over Load
GUP	Generation Unit Problem
DLOL	Distribution Line Over Load
PTOL	Power Transformer Over Load
OP	Operational (Intentional)
TLOL	Transmission Line Over Load
B.O.	Blackout

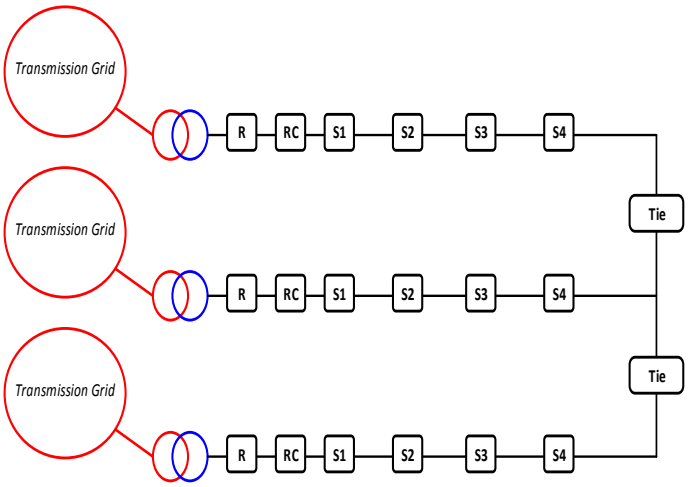

Fig. 7: Model of proposed Automated Feeder

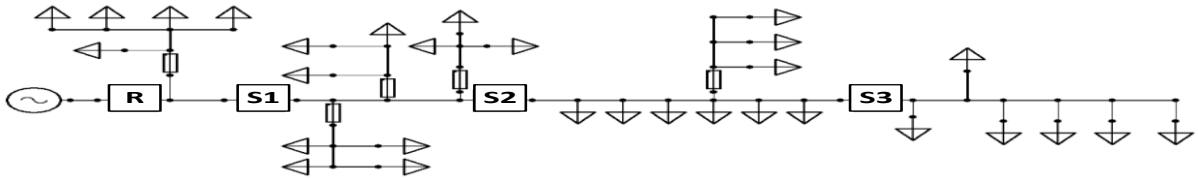

Fig. 8: Single line diagram of a Feeder Obtained using TELARM

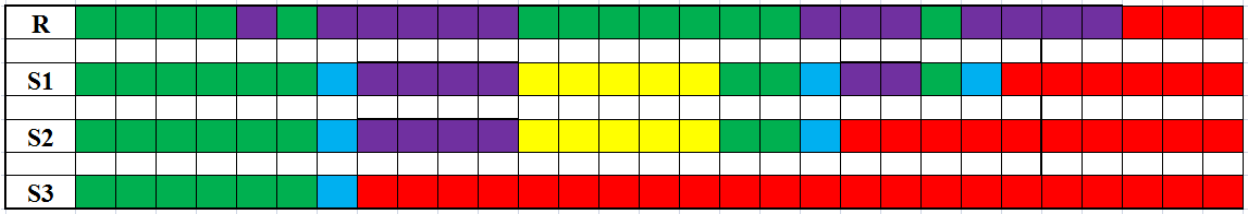

Fig. 9: Simulation result: State of Recloser and Sectionalizers under permanent fault at section 3

(Green indicates closed position, violet indicates open position, blue indicates tripping time, yellow indicates reclose time and red indicates open & lockout)

Table 3: Comparison of reliability indices of the existing feeder and the proposed automated system

No.	Reliability Index	Average standard reliability indices of the existing feeder system	Average standard reliability indices of the proposed model
1.	Annual SAIDI (hrs.)	21.67	5.611
2.	Annual SAIFI (no.)	30.22	3.117

CONCLUSIONS

The reliability analysis of the existing Addis Ababa distribution system reveals that around 55% of the total number of power interruptions are due to distribution system related problems and the rest 45% are due to others like generation, transmission problems and operational interruptions. Similarly, around 46% of the total duration of interruptions are caused by distribution system related problems and the rest 54% are due to the others.

Thus, it is observed that majority of the power interruption problems are related to the existing distribution system network. The effectiveness and potential benefits of implementing distribution system automation, specifically feeder automation to the distribution network of Addis Ababa, is investigated through simulation studies of the existing distribution system with proposed automation. The simulation results presented in Table 3 reveal that with the proposed distribution system automation, the system average duration index SAIDI) is improved by more than 69% and the system average frequency index (SAIFI) is improved by more than 88% as compared to those of the existing distribution system. These results clearly demonstrate that the system automation is capable of potentially mitigating the frequent interruptions and outage problems occurring in the existing Addis Ababa distribution system.

REFERENCES

[1] Oliver Schroedel, Michael Schwan, Sven Koeppe, Robert Rosenberger, "*Distribution Automation Solutions-Impact on System Availability in Distribution Networks*", CIRED International Conference on Electricity Distribution, June 2011.

[2] "Building Smart Grid for Smart Cities", ieema Journal, Volume 6, Issue No. 12, August 2015.

[3] Palak Parikh, Ph.D. Scholar "*Distribution System Automation"*, Electrical and Computer Engineering Department, University of Western Ontario, 2011.
[4] "*Smoothing the Rocky Road to Distribution Automation"*, Case Study, Motorola, 2010.
[5] James Northcote-Green Robert Wilson, "*Control and Automation of Electrical Power Distribution Systems",* Taylor and Francis Group, 2007.

[6] "*Evaluation of Representative Smart Grid Investment Grant Project Technologies: Distribution Automation"*, Pacific Northwest National Laboratory, February 2012.
[7] Ethiopian Electric Utility, Data Source: Strategic Management and Programming Office.
[8] "*Directives on Overhead Electric Line Clearances and Quality of Supply*", Ethiopian Electricity Agency, Addis Ababa, 2005.
[9] Turan Gonen, "*Electric Power Distribution Engineering*", third edition, CRC Press Taylor and Francis Group, January 2014.

Control Chart Pattern Recognition of Multivariate Auto-correlated Processes Using Artificial Neural Network

Birhanu Beshah and Ashenafi Muluneh
School of Mechanical and Industrial Engineering, Addis Ababa Institute of Technology, Addis Ababa University, Addis Ababa, Ethiopia
Email: birhanu.beshah@aait.edu.et

Abstract

The objective of this study is to model a control chart pattern recognition method for multivariate auto-correlated processes. The model development process uses a multi-layer feed forward Artificial Neural Network (ANN) architecture governed by back-propagation learning rule to identify and classify a set of sub-classes of abnormal patterns. Network training was conducted using simulated Control Chart Patterns (CCP) with Monte-Carlo simulation technique. A total of 3500 CCP examples (500 CCPs for each type of pattern) were generated and all CCPs data are normalized (standardized) before being employed as input to the neural network for better performance of the network. With this the study proposes a model for control chart pattern recognition of multivariate auto-correlated statistical process control to identify and classify seven types of typical control charts patterns: i.e. normal, downward shift, upward shift, decreasing trend, increasing trend, cyclic, and systematic patterns. The proposed framework is effective in control chart pattern recognition of multivariate auto-correlated processes with 94.9% recognition accuracy. Furthermore, the Control Chart Pattern Recognition (CCPR) model is validated by the data which is obtained from in-control process of a factory producing Alcohol and Liquor which demonstrates the accuracy of the CCPR. Pattern recognition for multivariate processes is common in the literature. But, this study proposed a new model for multivariate auto-correlated processes.

Key Words: *Multivariate Statistics, Control Chart, Neural Network, Process control*

Introduction

Control charts developed by Shewhart (1924) have been widely used in the quality control of manufacturing processes. They are still one of the most important tools of statistical process control. They are also useful in determining whether a process is behaving as intended or if there are some unnatural causes of variation. A process is out of control, if a point falls outside the control limits, or a series of points exhibit an abnormal pattern. These abnormal patterns provide important information regarding opportunities for process improvement. The presence of abnormal patterns indicates that a process is affected by assignable causes, and corrective actions should be taken (El-Midany et al., 2009). Therefore; identifying or analyzing abnormal patterns and diagnose the causes of out of control conditions are an important aspect of statistical process control. However, most of the studies in the pattern recognition of control charts emphasized on the pattern recognition of a single process variables or individual process variables (Chen & Zhou, 2009; Guh & Hsieh, 1999).

In many quality control settings, the manufacturing process may have two or more quality characteristics or quality variables to be controlled and monitored. The conventional practice in monitoring and controlling process variables has been to maintain a separate chart for each quality characteristic.

Individual process variable monitoring would result in some false out-of-control alarms when the characteristics are highly correlated, especially when one variable is dependent on the other and the correlations between variables result in degrading the statistical performance of the charts (Montgomery, 2009).

Multivariate Statistical Process Control (MSPC) is a set of techniques to deal with correlated variables. Commonly used techniques are Hotelling's T^2 chart, Multivariate Exponential Weighted Moving Average (EWMA) and Multivariate Cumulative Sum (MCUSUM) charts (Montogomery, 2009). Among these methods, Hotelling's T^2 chart is extensively applied in practice. However, dealing with multivariate data under the influence of auto-correlation requires additional considerations or modifications in designing the control schemes so as to ensure the control schemes are valid and robust; otherwise false alarm rate in the controlling process will appear (Hwarng & Wang, 2010). In the implementation of MSPC, control chart pattern recognition is the most important step in the process.

Different rules and methods have been developed to detect abnormal control chart patterns –runs test, zone test, geometric moving average test, and recently artificial neural network. The first three rules or tests indicate the presences of unnatural pattern in the process, but do not explicitly show the type of patterns (Hachicha & Ghorbel, 2012). Recent development in the field is the application of artificial neural network which has a capability to learn control chart patterns from a noisy data and recall during the real application of pattern recognition processes. Therefore, various artificial intelligence approaches have been applied into SPC. Neural networks (NNs) have an excellent noise tolerance in real time, requiring no hypothesis on statistical distribution of monitored measurements (Yu & Xi, 2009).

In a normally distributed univariate process data control chart pattern recognition using artificial neural network has been widely applied (Guh & Hsieh, 1999; Cox, 2005; Zobel, 2004; Addeh et al., 2011; Wang et al., 2008; Hwarng & Wang, 2010; and Salehi et al., 2012). In spite of its utility, research in the field of control chart pattern recognition of multivariate processes is limited. Wang and Chen (2002) proposed a neural fuzzy model for detecting mean shifts and classifying their magnitude in multivariate process. Salehi et al, (2011) proposed a hybrid learning-based model for on-line analysis of out-of-control signals in multivariate manufacturing processes. Zorriassatine, (2003) has developed a model for identification of abnormalities caused by mean shifts in bivariate process. El-Midany et al., (2010) proposed a framework to recognize a set of sub- classes of multivariate abnormal pattern (only for the pattern types of shift and trend), identify the responsible variables and classify the abnormal pattern parameters.

Their model used T^2 statistics (values) of the process variables as an input to their model structure of ANNs to recognize selected sub-classes of multivariate abnormal patterns in the process data. A survey on control chart pattern recognition by Hachicha & Ghorbel (2012), however, shows that there is no research made on multivariate auto-correlated process for detecting the types of abnormal patterns and pinpointing the variable or group of variables source that cause the out-of-control signal in more realistic processes. The purpose of this paper is to develop a control chart pattern recognizer model using an Artificial Neural Network for manufacturing industries with multivariate auto-correlated processes.

Research Methodology

In order to achieve the objective of this research, first, a control chart pattern recognition model using an artificial neural network was designed; second, the seven patterns were defined and the network has been trained and tested with simulated data; and third, the control pattern recognition model has been validated by taking a real data from a processing industry. A software package MATLAB® R2013a was used for designing and training the neural network, and also for generating MATLAB code of CCPR

procedure and running the application to evaluate process data. Monte-Carlo simulation technique was used for generation of example control chart patterns, and for training and testing the neural network.

During the pattern generation, a programming code was coded on python programming file, and 'Enthought Canopy®' was used to run the program file. In addition, the pattern generation was supported by a 'Spread sheet'.

Minitab 17® was used to standardize the simulated training data set and real process data which helps the neural network for better training performance, and also statistics like distribution estimation and auto-correlation coefficient determination of the collected process data has been done through Minitab.

Furthermore, Qualstat® software is applied for plotting multivariate T^2 control chart of the process data to ensure that the process is in control, which is used for comparison during the validation process of the result of the proposed CCPR model against the in-control process data.

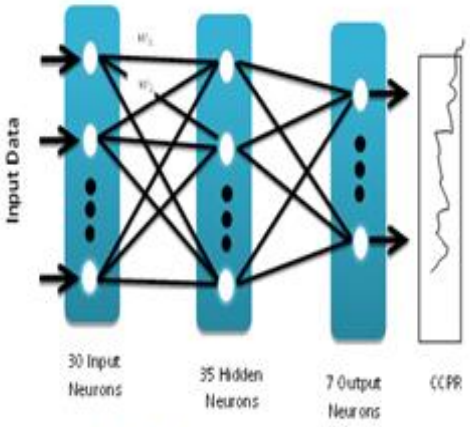

Figure.1 The Network Architecture

Artificial Neural Network Modeling

The neural networks proposed for this research are multilayer feed forward networks governed by back-propagation learning algorithm. It consists of three layers comprising input, hidden, and output layers. The number of input and output nodes was designated by the total number of inputs required to successfully represent a specified pattern and the number of pattern classes to be identified respectively.The input layer comprises 30 neurons which are used to put in 30 data (one control chart pattern example), these are taken from T^2 values of 30 consecutive observations (i.e. window size) in a control chart to the network. The seven (7) neurons in the output layer yield the type of the input pattern vector. The hidden layer consists of 35 neurons.

Although the more hidden neurons provide the better learning results, previous studies show that increasing hidden neurons could not improve the learning results, but will increase the total learning time. In this research, the hidden neuron was determined through trial and error; therefore, once the number of hidden neurons exceeds 35, it is not helpful for learning results. The input layer, hidden layer, and output layers are fully connected, and the connection weights are determined through the learning process. The network architecture adopted in this study is demonstrated in Figure 1. Additional parameters and features of the neural network design are summarized below: Let $X = \{x_1, x_2, \ldots, x_I\}$ be an arbitrary input sample vector, $Z = \{z_1, z_2, \ldots, z_O\}$ be the actual output vector, $D = \{d_1, d_2, \ldots, d_O\}$ be the desired output vector, $w_{ij}\ (1 \le i \le I,\ 1 \le j \le H)$ be the connection weight values between the input and hidden layers, $v_{jk}\ (1 \le j \le H,\ 1 \le k \le O)$ be the values between the hidden layer and the output layer, $\theta_j\ (1 \le j \le H)$ be the output threshold of each neuron in the hidden layer.

Activation or transfer function: Sigmoid transfer function is employed for both hidden and output layers. This function is frequently used in neural network applications primarily due to its function features, its continuous derivatives, and its insensitivity to noise (Hwarng and Hubele, 1993 and Perry et al., 2001).

This function is mathematically expressed as: $Y = f(I) = \frac{1}{1+e^{-\alpha I}}, 0 \le f(I) \le 1$, where α is the learning rate (α=0.01)

Error function: The mean square error (MSE) is used.

Initial connection weight and Learning rate: Initial connections weights are set in the range [-1, 1]. The learning rate α is the most important parameter. It scales the magnitude of weight adjustments and, thus can dramatically affect the rate of learning. In this study it is set at 0.01.

Training algorithm: When training large networks, and when training pattern recognition networks, scaled conjugated gradient learning algorithm is preferred since memory requirements are relatively small, and yet much faster than standard gradient descent algorithms. As an illustration of how the training works, consider the simplest optimization algorithm gradient descent. It updates the network weights and biases in the direction in which the performance function decreases most rapidly, the negative of the gradient. One iteration of this algorithm can be written as: $W_{ij}^{k+1} = W_{ij}^{k} - \alpha * Xi$, when output is increased from the target value and $W_{ij}^{k+1} = W_{ij}^{k} + \alpha * Xi$ when the output is decreased from the target value; otherwise $W_{ij}^{k+1} = W_{ij}^{k}$. Where, W_{ij}^{k+1} is the new adjusted weight, W_{ij}^{k} is the old weight, Xi is the input value, and α is the learning rate. This equation is iterated until the network converges.

Learning termination conditions:
The training of the Backward Propagation Network (BPN) is terminated when they reach a predetermined learning number or if the error does not improve in consecutive 6 epochs. In this study, the maximum learning number of BPN is set to be 1000.

Pattern Generation

In the real application of the result of this study the T^2 value obtained from the process data will be used as an input to the network in order to identify and/or classify abnormal patterns in the process. Therefore, the data generated has a univariate data value in which different data noises that can exhibit various abnormal patterns is introduced in order to imitate the real time patterns of process data. This simulation of various types of control chart patterns is useful for training the neural network so that the neural network can detect and/or classify patterns during the real time application of the neural network.

In generating such complex and large data, Monte-Carlo simulation technique is an efficient method. Pattern generation in several previous works of neural network approaches to control chart pattern recognition tasks has been successfully accomplished by the process mean and two noise components (eq. (1)).

$$X(t) = \mu + r(t) + d_t \qquad (5)$$

Where, $X(t)$ is the observation at time t, μ represent a known process mean of the data series when the process is in control, $r(t)$ is a random normal noise or variation (it is taken as being a random number in the range between -3 and 3, and d_t is a special disturbance due to some assignable cause.

The following expressions were used to generate data sets for the special disturbance due to some assignable causes of the different patterns of a control chart. Together with the normal pattern, this study addresses seven types of control chart patterns including normal, upward shift, downward shift, increasing trend, decreasing trend, cycle, and systematic pattern.

All the detail consideration for the generation of d_t of all the abnormal control chart patterns are expressed below: Notably, a normal pattern is one in which only common cause variations (background noise) are present in the control chart so that the process is considered to be in control.

Normal pattern
$d_t = 0$;

Upward Shift Pattern
$d_t = u * s$eq.
(6)
Where, u represents parameter to determine the position of shifting;

$u = \begin{cases} 0, & beforeshifting \\ 1, & aftershifting \end{cases}$ $s$is a shift magnitude

$(1.0 \leq s \leq 3.0)$.

Down ward Shift Pattern

$d_t = u * s$the same as the upward shift, however the shift magnitude has negative value.

$u = \begin{cases} 0, & beforeshifting \\ 1, & aftershifting \end{cases}$ $s$is a shift magnitude

(-3.0 ≤ s ≤-1.0).

Table1 : Parameters of Generated Process Data

Types of Control Chart Pattern	Parameters	Descriptions of patterns	Quantity generated
Normal		In control process data μ=0 & σ=1	500
Downward shift	$s =$ (-3.0 ≤ s ≤ -1.0)	Shift magnitude from process mean	500
Upward shift	$s =$ (1.0 ≤ s ≤ 3.0)	Shift magnitude from process mean	500
Decreasing trend	$\theta =$ (–0.30 ≤ θ ≤ –0.10)	Slope	500
Increasing trend	$\theta =$ (0.10 ≤ θ ≤0.30)	Slope	500
Cyclic	$k =$ (1.0 ≤k ≤3.0), $T = 10$	Amplitude, Period	500
Systematic	$a =$ (1.0 ≤ a ≤3.0)	Magnitude of process fluctuation	500

Increasing trend pattern

$d_t = \theta * t$ (7)

Where, θ represents trend slope taken as being in the range and t is time of observation.

Decreasing trend pattern

$d_t = \theta * t$

Here in decreasing trend, θ the trend slope has negative value (–0.30 ≤ θ ≤–0.10).

Cyclic pattern

$d_t = k * \sin(\frac{2\pi t}{T})$

(8)

Where, k represents cycle amplitude taken as being in the range (1.0 ≤k ≤3.0);

$T$is the cycle period in this research it is fixed at $T = 10$; and$t$ is the time of observation.

Systematic pattern:

$d_t = a * (-1)^t$eq. (9)

Where,a is the magnitude of the systematic pattern it is taken as being (1.0 ≤ a ≤3.0), determining the fluctuations above or below the process mean and$t$ is the time of observation.

To simulate the control chart patterns using Monte-Carlo simulation technique, first, control chart pattern generation program were coded on python program. Enthought Canopy® Software was used to run the python code. The data generated by the python program was used for training and the performance of the neural network could not be improved above 85% of successful classification of the testing sets. Therefore, in order to improve the network performance additional new data were generated using Microsoft Excel® (Spread Sheet).

A special cause disturbance for both upward and downward shift has been introduced at the middle of the recognition window. The summary of pattern parameters used for data generation is described in Table 1.

Network Training

Once the network has been designed, the network is trained (by optimizing the error function). This process determines the best set of weights and biases for training data set. In the training process of the network module, a total number of 3500 control chart training examples were used. Each types of pattern consists of an equal number of training examples, 500 control chart pattern examples for each type of abnormal patterns including a normal pattern. All the generated data are standardized (scaled) for better performance of the network training. During the training of the ANN CPR model the following methodology was implemented.

1) Data generated using Monte-Carlo simulation technique. 2) The generated data will be standardized for better performance of the neural network.3) Divide samples into training set (70%), validation set (15%) & testing set (15%) in random fashion. 4) Conduct the training on the designed ANN. 5) Validate the training using validation data sets, If the intended training goal is not met, go the next step, or else go back to train by adjusting the connection weights (an epoch). 6) During the training when the network performance

goal is met, test the trained network using testing data set. If the result is acceptable, finalize the training and trained ANN is ready for use; otherwise go back to modify the network or increase and/or change the training data set. In this training, the output calculation, back-propagation and updates of weight is conducted. The initial connection weights, the learning rate, and momentum factor of the back-propagation network are set to the MATLAB's standard configuration of the training rules. All the training examples were presented to the neural network in a random fashion. The desired outputs for the network are defined by the following categories as shown in Table 2. Table 3 summarizes the classification results of the proposed control chart pattern recognition model on the testing example set using a confusion matrix that shows the distribution of the misclassification. Here, a type I error occurs when a normal testing control chart pattern example is wrongly predicted (classified) as an abnormal control chart pattern by the proposed control chart pattern recognition model. A type II error occurs when an anormal testing control chart pattern example is wbrongly classified as a normal control chart pattern by the proposed model. For instance, for the normal pattern, the type I error of the proposed model was 10.4%, while the type II errors were 2.7%, 2.7%, 0.0%, 0.0%, 0.0%, and 0.0% for pattern types of downward shift, upward shift, decreasing trend, increasing trend, cycle, and systematic respectively. Most of the misclassification was observed to happen in the recognition of downward shift, upward shift, and increasing and decreasing trend patterns. With the presence of downward shift patterns, most of the misclassified patterns are classified as decreasing trend and less frequently as a normal pattern. In the presence of upward shift patterns, most misclassifications were classified as increasing trends and less frequently as normal patterns. In increasing trend patterns all of misclassifications were upward shift patterns, whereas in decreasing trend all misclassifications were a downward shift pattern. The misclassification between shift and trend patterns indicates that patterns with small shift magnitudes resemble with trend patterns and vice versa. Both cyclic and systematic patterns were not misclassified. The overall testing result (94.1%) indicates that the training was successful and the neural network performance is accurate.

Model validation

Multivariate statistical process control using residual hotelling T^2 control chart is integrated with the proposed control chart pattern recognition model to make the process monitoring and controlling activity effective. Data will be taken from the online manufacturing process and T^2 control chart plotted. If the process is in-control go to the next process monitoring. If the process is out of control the T^2 values of the observed data standardized and input to CCPR model to determine an abnormal pattern. If there is an abnormal pattern, with good process knowledge the assignable cause will be diagnosed and online action will be taken to the manufacturing process. If the result from the CCPR is normal pattern, the process is out of control because of an outlier/s. Therefore, the possible assignable causes will be diagnosed with good process knowledge; otherwise further action for diagnosing the assignable cause will be conducted by using MYT decomposition method or principal component analysis. Validation of the control chart pattern recognition model based on data collected form a company processing Alcohol and Liquor products. Characteristics which are serially dependent determine the successful outputs of the manufacturing process. The production process of alcoholic liquor involves several sequenced processes starting from molasses several process variables and quality syrup preparation up to liquor packaging and distributing. Previous studies conducted in process monitoring and controlling indicates that there are 20 critical process variables and quality characteristics in the production process (Lemma, 2014). These process variables and quality characteristics are described in **Table 4**. These process variables (multivariate auto-correlated process variables) are serially dependent and exhibit correlation either strongly or moderately among each other. For the purpose of this research, 93 sample data were collected from each type of process variables and quality characteristics as seen in **Table 5**. These data were processed and presented to the control chart pattern recognizer model to identify the

types of patterns exhibited from this collected data. At the early stage of the process monitoring and controlling, the collected auto-correlated data treated for removal of auto-correlation using time series predicting model and then using this predicted data T^2 control chart is developed.

Table 2: Representation of Output Categories

Control chart pattern type	Outputs category						
	1	2	3	4	5	6	7
Normal	1	0	0	0	0	0	0
Downward shift	0	1	0	0	0	0	0
Upward shift	0	0	1	0	0	0	0
Decreasing trend	0	0	0	1	0	0	0
Increasing trend	0	0	0	0	1	0	0
Cyclic	0	0	0	0	0	1	0
Systematic	0	0	0	0	0	0	1

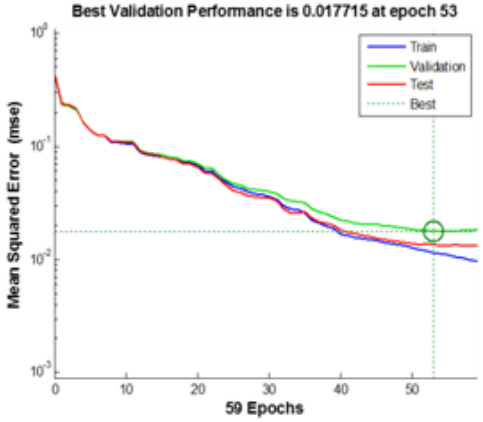

Figure 2: The network Training Performance

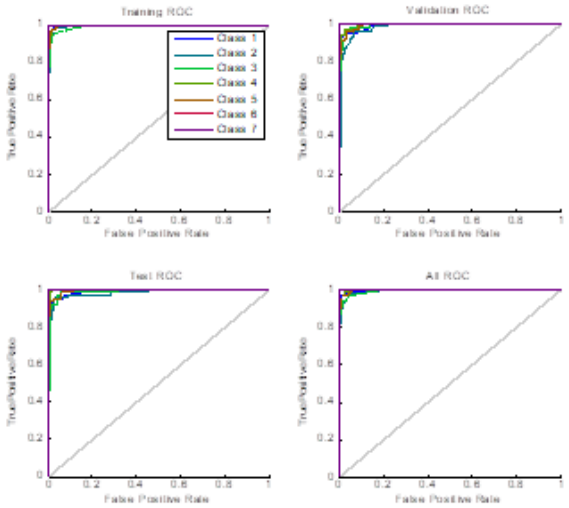

Figure 3: Network Training Receiver Operating Characteristics (ROC) Curve

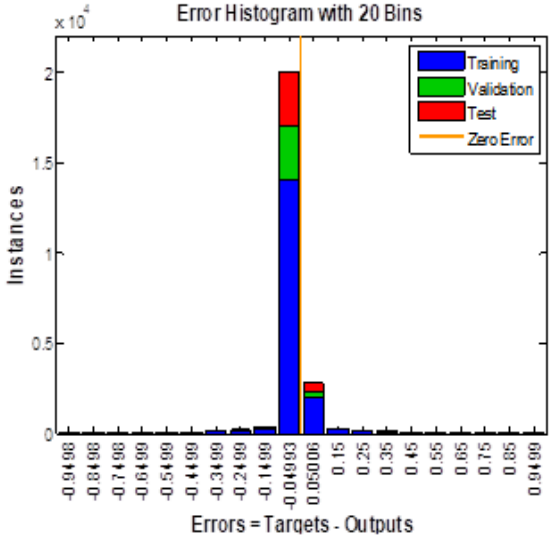

Figure 4: Error Histogram

Table 3: Matrix Showing the Classification of the Testing

		Predicted pattern						
	Types of patterns	Normal	Downward shift	Upward shift	Decreasing trend	Increasing Trend	Cyclic	Systematic
True Patterns	Normal	89.6%	5.97%	2.98%	0	1.49%	0	0
	Downward shift	2.7%	90.5%	0	6.76%	0	0	0
	Upward shift	2.7%	0	91.9%	0	5.4%	0	0
	Decreasing trend	0	6.4%	0	93.6%	0	0	0
	Increasing Trend	0	0	7.14%	0	92.86%	0	0
	Cyclic	0	0	0	0	0	100%	0
	Systematic	0	0	0	0	0	0	100%

Table 4: Critical Process Variables and Quality Characteristics

Process/stage	Variable	Variables Representation
1.Fermentation process	Fermented wine Brix	FWB
	Fermented wine temperature	FWT
	Fermented wine GL	FWGL
2. Distillation process	Fermented wine feed rate	FWFR
	Rectification column temperature	RCLT
	Pre-heater column temperature	PHCLT
	Fusel oil column temperature	FOCLT
	Filter column temperature	FCLT
	Rectification condenser temperature	RCNT
	Fusel oil condenser temperature	FOCNT
	Acidity condenser temperature	ACNT
	Distillation condenser temperature	DCNT
	Filter condenser temperature	FCNT
	Rectification column reflux rate	RCLR
	Fusel oil column reflux rate	FOCLR
	Filter column reflux rate	FCLR
3. Pure alcohol product	Pure alcohol extraction rate	PAE
	Pure alcohol grade	PAG
	Permenganent time	PT
4.Liquor product	Liquor Grade	LG

Table 5: Collected Data for 20 Critical Variables of NALF

Obsv No.	FWB	FWT	FWGL	FWFR	.	.	.	FCLR	PAE	PAG	PT	LG
1	7.3	31.8	6.0	3200.0	.	.	.	300.0	237.4	96.4	2.5	39.6
2	7.3	30.5	5.5	3200.0	.	.	.	300.0	237.4	96.4	2.5	39.9
3	7.3	31.5	7.0	3200.0	.	.	.	280.0	240.0	96.4	2.5	39.8
4	7.7	31.0	6.8	3200.0	.	.	.	370.0	233.2	96.4	2.5	40.2
.	.	.	.	.	.	.	.	.	.	.	.	.
.	.	.	.	.	.	.	.	.	.	.	.	.
.	.	.	.	.	.	.	.	.	.	.	.	.
90	8.9	32.5	7.5	3200.0	.	.	.	420.0	230.0	96.5	2.0	40.2
91	8.2	31.0	7.5	3200.0	.	.	.	440.0	220.0	96.5	2.0	39.8
92	9.1	33.5	7.5	3200.0	.	.	.	440.0	220.0	96.5	2.0	39.9
93	8.2	33.0	7.5	3200.0	.	.	.	440.0	230.0	95.0	2.0	40.4

Table 6: T^2 Values of the Collected Process Data

	Observation No.	T^2 Values (data1)	Observation No.	T^2 Values (data2)	Observation No.	T^2 Values (data3)
Control chart Pattern Recognition Window	1	20.81035	31	12.81919	55	21.30466
	2	21.80719	32	11.43592	56	25.91325
	3	26.90726	33	12.42666	57	28.7044
	4	19.40346	34	12.49176	58	22.19562
	5	16.33248	35	10.13335	59	13.31291
	6	16.36439	36	9.989161	60	7.240752
	7	37.21674	37	14.63964	61	11.52447
	8	33.8086	38	15.45348	62	20.90234
	9	32.18515	39	15.52241	63	7.983093
	10	15.16282	40	23.63752	64	22.81666
	11	22.83228	41	18.64971	65	27.13319
	12	17.99016	42	17.27818	66	12.43383
	13	22.50832	43	26.66137	67	14.50844
	14	21.21474	44	28.48098	68	18.51175
	15	31.52029	45	18.72264	69	11.88646
	16	29.44914	46	23.96568	70	12.32784
	17	37.62803	47	13.50697	71	16.71864
	18	26.15612	48	16.74802	72	12.77594
	19	20.0743	49	20.04498	73	20.10003
	20	12.48489	50	17.62342	74	22.74139
	21	25.66959	51	14.25	75	26.10231
	22	18.47132	52	23.67614	76	14.4545
	23	19.55558	53	18.94915	77	17.72669
	24	34.93054	54	15.65261	78	9.51546
	25	25.52647	55	21.30466	79	26.9718
	26	18.4959	56	25.91325	80	10.80547
	27	26.8129	57	28.7044	81	20.8425
	28	12.57247	58	22.19562	82	9.103688
	29	18.4959	59	13.31291	83	15.74605
	30	26.8129	60	7.240752	84	11.73663

From this data, the T^2 values are used as an input to the neural network model developed, to identify and classify the control chart patterns exhibited by the collected process data. The T^2 values of the collected process data are listed in Table 6. To apply the

proposed model, the T^2 values of the collected data are calculated (**Table 2**.), that is obtained from hotelling's T^2 control chart of a controlled process was taken and standardized to values (μ=0, σ=1), and presented to the neural network control chart pattern recognizer. The trained network starts to recognize the type of pattern exhibited by the data presented based on the window size of 30 consecutive observations and the output of the recognition is presented as follows:

The size of recognition window (window length) can significantly affect the performance of the control chart pattern recognizer (Lin et al., 2011 and Guh & Shiue, 2008). The window length is defined as the number of sample points to be considered at a time in detecting an unnatural pattern. Since the number of network inputs affects the size of the network, emphasis should be given to the selection and representation of the data in the training set. For quick computation in process control, lesser window size is efficient; however, as previous studies indicated, too small window size detects control charts quickly that means it has a shorter Average Run Length (ARL). This situation might generate higher Type I error due to insufficient information to represent the features of data. On the other hand, if the window size is too large, it might generate higher Type II error and may consume significant computation time. In this study, a window size of 30 were selected through trial and error in order to obtain good generalization performance of the neural network. The T^2 control chart which shows the in control process generated by Qualstat software application was presented in **Figure 5**. As it is seen in the control chart, all the data points are distributed below the upper control limit of the process which shows the process being in control.

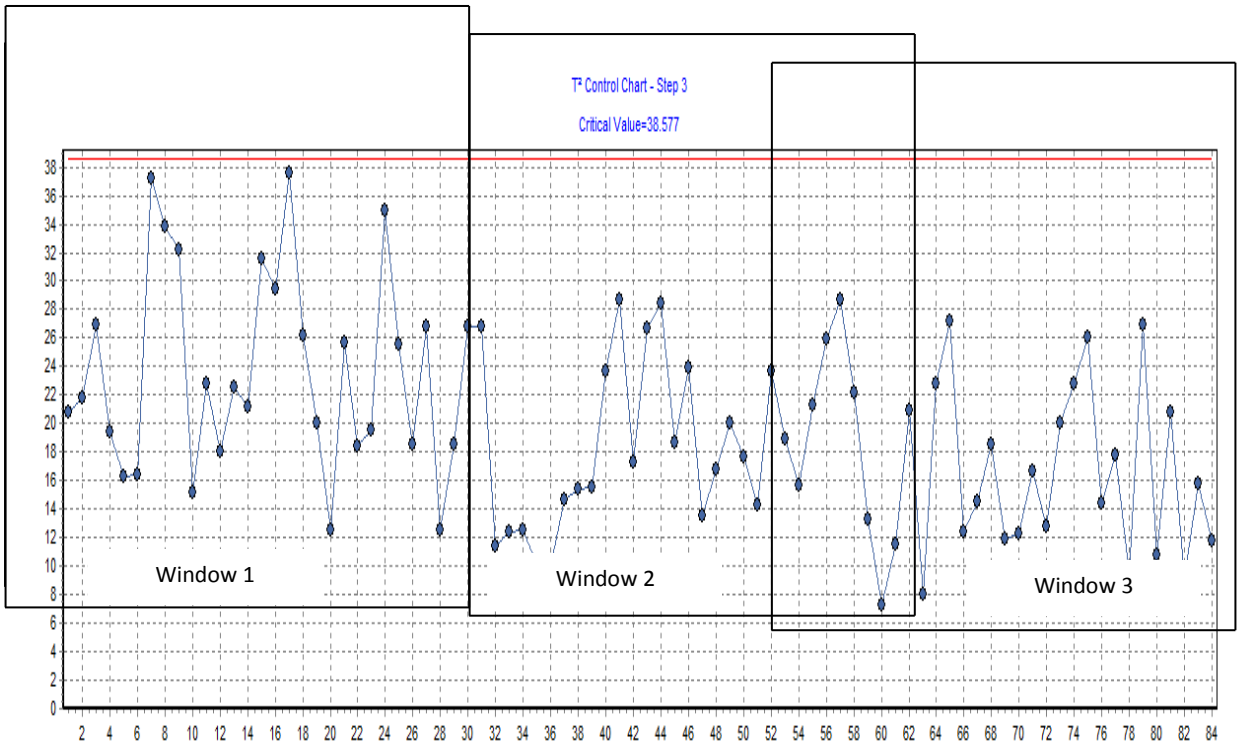

Figure 5 : T^2 Control Chart for Observations

As any window of data is applied to the trained network, one of the predefined pattern classes (normal, downward shift, upward shift, decreasing trend, increasing trend, cyclic, and systematic pattern) is determined. In this aspect when the given observation of the above window sizes of the standardized T^2 values for observation No. 1-30 (data1), 31-60 (data2), and 55-84 (data 3) are applied in a separate window to the proposed CCPR, the following output were identified: The control chart pattern recognition model classifies all the three control chart patterns presented from the in control process as a normal pattern. Therefore, this result shows that the control chart pattern recognition model performs very accurately by generating the same results with the predefined state of the process.

CONCLUSIONS

The training result shows that, the neural network has a very good performance in recognition of control chart patterns with overall recognition accuracy of 94.9%. In the network testing results, it was observed that most of the misclassification to happen in the recognition of downward shift, upward shift, and increasing and decreasing trend patterns. With the presence of downward shift patterns, most of the misclassified patterns are classified as decreasing trend and less frequently as a normal pattern. In the presence of upward shift patterns, most misclassifications were classified as increasing trends and less frequently as normal patterns. In increasing trend patterns all of misclassifications were upward shift patterns, whereas in decreasing trend all misclassifications were a downward shift pattern. The misclassification between shift and trend patterns indicates that patterns with small shift magnitudes resembles with trend patterns and vice versa. It is also found that both cyclic and systematic patterns were not misclassified (recognized with 100% accuracy). From the presented testing data though there are both type I type II errors, the overall testing result (94.1%) indicates that the training was successful and the neural network performance is accurate. The proposed methodology was evaluated using the controlled process data from a company process and accurate results were obtained as the control chart pattern recognition model signals an output of a normal control chart pattern. This result shows that the integration of control chart pattern recognition model and multivariate statistical process control technique can give a better performance of process monitoring and controlling activity.Hence, the proposed model can be adapted to various process settings of manufacturing industries. In the adoption of the model proposed by this study to reduce the misclassification rate among different classes of control chart patterns, one should increase the number of training examples with those patterns that exhibit higher confusion rate in this study. In the application and effective use of this model, manufacturing industries should also determine the possible association of assignable causes with specific control chart pattern exhibited by their process.Further research shall be done on the magnitude of special cause disturbance like shift magnitude, trend slope, cycle amplitude and period, and process fluctuation magnitude that are important activity in control chart pattern recognition, the task of estimation of this parameter magnitudes were not included in this study. This study considers seven types of control chart patterns. Hence, future study shall also address the situations when multiple (mixed) abnormal patterns exist concurrently in multivariate process control charts.

REFERENCES

1. Adugna Lemma, (2014); Monitoring and Controlling Multivariate Process of National Alcohol and Liquor Factory, Masters Thesis, Addis Ababa Institute of Technology, Addis Ababa.
2. Chih-Hsuan Wang, Ruey-Shan Guo , Ming-Huang Chiang &Jehn-Yih Wong (2008) Decision tree based control chart pattern recognition, International Journal of Production Research, 46:17, 4889-4901
3. Christopher W. Zobel, Deborah F. Cook & Quinton J. Nottingham (2004), An augmented neural network classification approach to detecting mean shifts in correlated manufacturing process parameters, International Journal of Production Research, 42:4, 741-758
4. Douglas C. Montgomery (2009); Introduction to Statistical Quality Control, sixth edition, John Wiley & Sons, Inc.
5. El-Midany, T. T., El-Baz, M. A., &Abd-Elwahed, M. S. (2010). A proposed framework for control chart pattern recognition in multivariate process using artificial neural

networks. Expert Systems with Applications, 37(2), 1035–1042
6. Hwarng, H. B., & Wang, Y. (2010). Shift detection and source identification in multivariate autocorrelated processes. International Journal of Production Research, 48(3), 835–859.
7. Hwarng, H.B., 2004. Detecting process mean shift in the presence of autocorrelation: a neuralnetwork based monitoring scheme. International Journal of Production Research, 42 (3), 573–595.
8. JalilAddeh,AtaEbrahimzadeh&VahidRanaee (2011), Control Chart Pattern Recognition Using Adaptive Back Propagation Artificial Neural Networks and Efficient Features, 2nd ICCIA
9. Jianbo Yu &Lifeng Xi (2009) A hybrid learning-based model for on-line monitoring and diagnosis of out-of-control signals in multivariate manufacturing processes, International Journal of Production Research, 47:15, 4077-4108
10. M.A.A. Cox (2005), A Neural Network Method for Modelling the Parameters of a CUSUM Chart, Quality Engineering, 17:2, 197-205.
11. Marcus B. Perry , Julie K. Spoerre& Tomas Velasco (2001), Control chart pattern recognition using back propagation artificial neural networks, International Journal of Production Research, 39:15, 3399-3418
12. MATLAB R2013a Neural Network Tool Box.
13. MojtabaSalehi, Reza BaradaranKazemzadeh& Ali Salmasnia (2012), On line detection of mean and variance shift using neural networks and support vector machine in multivariate processes Applied Soft Computing 12 (2012) 2973–2984
14. Nan Chen &Shiyu Zhou (2009) Detectability study for statistical monitoring of multivariate dynamic processes, IIE Transactions, 41:7, 593-604
15. R. L. Mason, N. D. Tracy, and J. C. Young, 1995, Decomposition of T2 for Multivariate Control Chart, Interpretation Journal of Quality Technology, vol. 27, pp. 99-108, 1995.
16. R. L. Mason, Y.M. Chou, J. H. Sullivan, Z.G. Stoumbos, and J.C. Young; Systematic Patterns in T2 Charts. Journal of Quality Technology 35 (2003) 47-58.
17. R.-S. Guh& J.D.T. Tannock (1999) Recognition of control chart concurrent patterns using a neural network approach, International Journal of Production Research, 37:8, 1743-1765.
18. R.-S. Guh (2008), Real-time recognition of control chart patterns in autocorrelated processes using a learning vector quantization network-based approach, International Journal of Production Research, 46:14, 3959-3991.
19. Ruey-ShiangGuh&Yeou-RenShiue (2008) Effective Pattern Recognition Of Control Charts Using A Dynamically Trained Learning Vector Quantization Network, Journal of the Chinese Institute of Industrial Engineers, 25:1, 73-89
20. Ruey-ShiangGuh (2005), A hybrid learning-based model for on-line detection and analysis of control chart patterns. Computers & Industrial Engineering 49 (2005) 35–62.
21. Ruey-Shy Guh& Yi-Chih Hsieh, 1999. A neural network based model for abnormal pattern recognition of control charts, Computers & Industrial Engineering 36 (1999) 97 – 108.
22. Ruixiang Sun & FugeeTsung (2003) A kernel-distance-based multivariate control chart using support vector methods, International Journal of Production Research, 41:13, 2975-2989.
23. S. Sahran, (2007), Application of Spiking Neural Networks and the Bees Algorithm to Control Chart Pattern Recognition; A thesis submitted to Cardiff University, for the degree of Doctor of Philosophy.
24. Salehi, M., Bahreininejad, A., &Nakhai, I. (2011). On-line analysis of out-of-control signals in multivariate manufacturing processes using a hybrid learning-based model. Neuro computing, 74(12–13), 2083–2095.
25. Shih-Yen Lin, Ruey-ShiangGuh, Yeou-RenShiue, (2011); Effective recognition of control chart patterns in autocorrelated data using a support vector machine based approach; Computers & Industrial Engineering 61 (2011) 1123–1134
26. WafikHachicha& Ahmed Ghorbel, (2012). A survey of control-chart pattern-recognition literature (1991–2010) based on a new conceptual classification scheme. Computers & Industrial Engineering 63, 204–222.
27. Wenchang Chen, 2005, Master Thesis Multivariate Statistical Process Control in Industrial Plants, Delft University of Technology.
28. Zorriassatine, F. et al. (2003).Using novelty detection to identify abnormalities caused by mean shifts in bivariate processes. Computers & Industrial Engineering, 44, 385–408.

ACKNOWLEDGEMENTS

The Editorial Board of Zede Journal of Ethiopian Engineers and Architects would like to express its sincere gratitude to the following individuals for reviewing the manuscripts that were originally submitted for publication in Zede Volume: 35

Abreham Assefa(Dr.)
Abreham Gebre(Dr.)
Amare Mahtebu (Ing)
Deinammo Addise(Dr.)
Dereje Shiferaw(Dr.)
Esheite Berhan (Dr.)
Fekadu Shewarega(Dr.)
Gizachew Shiferaw (Ing.)
Hundessa Desalegn(Dr.)
Niguse Habtu(Dr.)
Mohammed Abdo(Prof.)
N.P.Singh(Prof.)
Temesgen Wondemu(Dr.)
Teshome Worku (Ato)